A Comparison of Anthropogenic and Long-term Soil Erosion on Banks Peninsula in the South Island of New Zealand, Using ^{137}Cs and Kawakawa Tephra

MASTER THESIS

submitted in partial fulfilment
of the requirements for the Degree of
Master of Natural Resources Management
and Ecological Engineering (M.Na.R.M.& E.E.)

A joint degree of

University of Natural Resources and Applied Life Sciences (BOKU),
Vienna, Austria,
and
Lincoln University (LU), Christchurch, New Zealand.

Submitted by

Franz Stephan LUTTER

Supervised by
O. Univ. Prof. Dr. phil. Florin Florineth (BOKU),
Senior Lecturer Dr. Peter Almond (LU)

Vienna, March 2007

Preface

The Master of Natural Resources Management and Ecological Engineering (MNaRMEE) is an innovative joint degree offered by the University of Natural Resources and Applied Life Sciences (BOKU), Vienna, Austria, and Lincoln University (LU), Christchurch, New Zealand. It focuses on the commitment to the sustainable use of natural resources from an international point of view. This allows for the enrichment and widening of the graduate's horizon, through providing the opportunity to compare experiences in contrasting environments. It has been thanks to this approach and to the people I had the opportunity to work with or got to know independently of my studies that this postgraduate experience has turned out to be so successful – on a professional as well as on a personal level. In this context, I would like to address special thanks to those who supported me generously in the accomplishment of my master thesis and degree, in New Zealand as well as in Austria.

First and foremost, I thank my supervisor at Lincoln University, Peter Almond, who imparted his knowledge of soil science and geomorphology with a lot of enthusiasm – and patience. His expertise and helpfulness laid the foundation for a successful completion of the thesis, and his personal commitment to our study was additional motivation for me.

Likewise, I owe a great debt of gratitude to my friends and colleagues of the Soil and Physical Sciences Group who supported me with a lot of experience, time and motivation; amongst others, especially Graeme Buchan, Amanda Clifford, Roger Cresswell, Leanne Hassall, Matthew Hughes, and Carol Smith.

I would not have been able to carry out the field work in the surroundings of the Ahuriri quarry, if it was not for the kindness of Mr. Greg Horgan, the owner of the property where the study transect was located. I owe him additional thanks for the background information concerning the cultivation history.

On the Austrian side, special thanks go to my supervisors Florin Florineth and Hans-Peter Rauch from the Institute of Soil Bioengineering (IBLB) at BOKU University who advised me in a very professional, cooperative and at the same time personal way.

I also would like to express my appreciation that BOKU University and Lincoln University enabled me to take part in this joint degree. Due to their awareness regarding the importance

of the internationalisation of environmental management, I have been given the opportunity to develop my skills for future use in generating sustainable lifestyles.

Last but not least, it is more than appropriate to thank my family and friends in Austria and New Zealand, for their encouragement in taking this opportunity of further education, and their support during my studies overseas. Without this background the realisation of this masters thesis as well as of the whole degree would not have been possible!

Kia ora!

Abstract

The task of the present study is to assess the severity of anthropogenically induced soil erosion, and hence the sustainability of the present land use, on a loess-mantled hillslope on the foothills of Banks Peninsula, in the South Island of New Zealand. The analysis is restricted to a slope segment representative for the soil creep-type processes that dominate on convex soil-mantled hillslopes which satisfy the assumptions of the soil erosion measurement techniques employed.

To quantify long-term (natural) and short-term (often anthropogenically induced) erosion rates tracers within the soil are used. The thickness of soil above a ca 26,500 year old tephra, and an inventory of the amount of that tephra are used to determine the long-term rate across a convex hillslope, from the interfluve to the midslope. An inventory of bomb-fallout ^{137}Cs is used to determine short-term rates over the same hillslope.

A slope dependent transport model is parameterised to encapsulate transport efficiency relevant to the short and long time scales, and the parameters are used as a basis for comparing soil erosion rates at different time scales. For the long-term erosion rate, the transport coefficient, capturing the efficiency of soil erosion, K_{long} is ~ 0.003 m^2 yr^{-1}. This result of the tephra analysis is slightly lower than the values determined in similar studies carried out in landscapes where a transition in the vegetation had occurred (Roering et al., 2002 and 2004; Walther, 2006).

Due to the variability in the ^{137}Cs data and to the little extent of erosion in the short time scale K_{short}, the short-term transport coefficient, cannot be determined. Nevertheless, there is no evidence to suggest that it is any greater than K_{long}, which would indicate an increase in soil erosion efficiency from the long to the short time scale. Despite the relatively stable conditions on the upper backslopes, on the lower backslope tunnel gullies are actively transporting sediment and this is probably the major locus of erosion in the landscape, requiring future research for its quantification.

Kurzfassung

Ziel der vorliegenden Arbeit ist es, das Ausmaß des menschlichen Einflusses auf Bodenerosion – und in weiterer Folge die Nachhaltigkeit der gegenwärtigen Bodennutzung – auf einem Löss-bedeckten Hang am Fuße der Banks Peninsula auf der Südinsel von Neuseeland abzuschätzen. Die Studie wurde dabei auf einen Hangabschnitt beschränkt, auf dem die für konvexe Hänge typischen Kriech-Prozesse vorherrschen, da diese die für die Messtechniken notwendigen Annahmen befriedigen.

Um langfristige (natürliche) und kurzfristige (vom Menschen verursachte) Erosionsraten zu quantifizieren, werden verschiedene Tracer im Boden verwendet. Über die Dicke des Bodens oberhalb einer 26.500 Jahre alten Asche-Schicht und die Quantifizierung dieser Asche wird die langfristige Erosionsrate bestimmt; die kurzfristige über die Quantifizierung und räumliche Verteilung des aus radioaktivem Niederschlag stammenden Elementes ^{137}Cs auf demselben Hang.

Ein Neigungs-abhängiges Transportmodell wird parametrisiert, um die lang- und kurzfristige Transportleistung auf dem untersuchten Hang zu beschreiben, beziehungsweise um die jeweiligen Transportraten vergleichen zu können. Für die langfristige Erosionsrate beträgt der Transportkoeffizient $K_{long} \sim 0{,}003\ m^2\ yr^{-1}$, was etwas unter den Werten liegt, die in ähnlichen Studien bestimmt wurden, die in Gegenden durchgeführt wurden, wo eine Veränderung hinsichtlich der Vegetationsbedeckung stattgefunden hatte (Roering et al., 2002 and 2004; Walther, 2006).

Aufgrund der Variabilität der ^{137}Cs-Daten und des geringen Ausmaßes an Erosion im kurzen Zeitmaßstab konnte der kurzfristige Transportkoeffizient K_{short} nicht ermittelt werden. Nichtsdestotrotz gibt es keinen Anhaltspunkt anzunehmen, dass K_{short} größer als K_{long} ist, was eine Zunahme der Bodenerosion bedeuten würde. Ungeachtet der relativ stabilen Verhältnisse im untersuchten oberen Bereich des Hanges ist am Hangfuß aktiver Sedimenttransport – „Tunnel-Gully-Erosion" – augenscheinlich, zu dessen Quantifizierung weitere Studien vonnöten sein werden.

TABLE OF CONTENTS

1 INTRODUCTION

1.1 Task and approach

The landscape of New Zealand, the majority of which was covered in forest, has changed significantly since the relatively recent arrival of humans. With the first Maori settlers (~ 700 years ago) the clearing of large areas of forest began, and accelerated after the arrival of Europeans 150 years ago. A consequence of this clearance has been an increase in the risk and severity of soil erosion. However, New Zealand is located on the boundary between the Australian and the Pacific Plate, and the deformation associated with the convergence occurring at this boundary has a strong influence on the development of the landforms in New Zealand; not only because of the resulting uplift (and as a consequence the creation of the axial ranges), but also because of the enormous erosion rates which are balancing this uplift. Furthermore, as a consequence of its latitude, New Zealand is exposed to glacial and periglacial erosion processes, particularly in glacial periods, and high rates of wind erosion.

In order to be able to assess the severity of anthropogenically induced soil erosion, it is necessary to quantify the natural rates of erosion – at short as well as long time scales. This quantification and the comparison of the resulting erosion rates from different time scales are the main components of this master's thesis.

The study is carried out on a loess-covered, convex-shaped hillslope on the foothills of Banks Peninsula. Convex soil-mantled hillslopes evolve through slope-dependent transport processes, for example through creep, resulting from disturbance by 1) expansion and contraction due to freeze-thaw, wet-dry and hot-cold cycles, 2) by biologic activity (Dietrich et al., 2003), or 3) – perhaps most significant for the current processes – by rain splash. The region has experienced climate changes and, consequently, changes in vegetation cover from forest to shrub vegetation and grassland (Shulmeister et al., 1999). It is the aim of the present study to discover if the present rate of soil erosion under introduced grassland is similar to or different from the long-term average rate, and to draw conclusions concerning the necessity of measures against present erosion processes.

Tracers within the soil can be used to quantify long-term (natural) and short-term (often anthropogenically induced) erosion rates. The thickness of soil above a ca 26,500 year old tephra, and an inventory of the amount of that tephra are used to determine the long-term rate

of erosion across a hillslope transect, from the interfluve to the midslope. An inventory of bomb-fallout ^{137}Cs is used to determine short-term rates (~ 40 years) over the same hillslope.

The loss of soil due to erosion, on the foothills of Banks Peninsula mainly caused by rain splash, pipe-tunnel erosion, creeping processes, or wind (Eyles, 1983), is problematic especially seen from a sustainability point of view. On the one hand soil is an important global resource for food, fibre, and timber production, as well as it is a habitat for fauna and flora, and on the other hand soil loss often causes hazardous events. The present study aims to prove to what extent cultivation and exploitation cause degradation of soil on Banks Peninsula, in order to enable a more sustainable soil management.

1.2 Literature review

1.2.1 Soil transport on soil-mantled hillslopes

On the foothills of Banks Peninsula, soil loss due to erosion is mainly driven by rain splash, pipe-tunnel erosion, creeping processes, and wind (Eyles, 1983). In the following, the main principles of different forms of detachment and transport will be explained more in detail.

Rain splash

Tschang (1972) describes "splash erosion" as "the erosive action of raindrops and/or water-drops in striking the earth's surface", and explains that the raindrops by impact destroy the soil structure, detach soil particles and favour the rainwash process. Farres (1978, as cited in Selby and Hodder, 1993, p. 225) distinguishes two types of detachment of soil particles: 'creep' (lateral displacement) and 'saltation' (splashing of soil particles in the air). The particles separate, and the infiltration rate of the soil becomes lower due to infiltration of fine particles into the pore space, building a 0.1-3.0 mm crust (Farres, 1978, as cited in Selby and Hodder, 1993, p. 225) and increasing the surface runoff, due to the decrease in permeability caused by the crust (Tschang, 1972).

The severity of erosion caused by raindrop impact depends very much on the amount, the intensity and the duration of a particular rainfall (erosivity) (Tschang, 1972; Selby and Hodder, 1993). According to the type of climate, the rainfall intensity can range from 75 mm h^{-1} (temperate climate) up to 340 mm h^{-1}; drops can reach a size of 5 mm and a velocity of 9 m s^{-1}. In addition, the resistance of a specific soil to raindrop erosion (erodibility) is strongly connected to its vegetation cover which performs an interception function. Therefore, land management plays an important role with regard to soil conservation.

Overland flow – wash erosion

Overland flow consists of interrill (sheet) and rill erosion, and can be divided into two types – Horton overland flow, and saturation overland flow (Parsons and Abrahams, 1992). The former takes place when surface infiltration rates are exceeded by the intensity of rainfall; the latter where soil gets saturated, for example in long storm events of low intensity. While saturation overland flow is to be found mainly on foot slopes marginal to stream channels, to topographic hollows and to areas of thin soil cover, Horton overland flow is typical on agricultural lands and in arid and semi-arid areas, where infiltration is limited due to bedrock outcrops and sparse vegetation cover leads to surface sealing. The total resistance to interrill erosion caused by overland flow is determined by grain resistance, form resistance, wave resistance, and rain resistance. Grain resistance involves the kinetic energy necessary to overcome the no-slip condition at the boundary, as well as the energy dissipated in separation eddies which are caused by particles and microaggregates protruding above the viscous sublayer. Form resistance is exercised, for instance, by stones or vegetation which cause energy to dissipate in separation eddies, secondary circulation and locally increased shear. Wave resistance is the energy loss caused by deformation of the free water surface, such as sudden flow decelerations at the base of local steepenings or between large roughness elements. Finally, rain resistance is described as the retardation of the flow velocity due to the transference of the flow momentum to accelerate the rain drop mass (Abraham et al., 1992).

Describing the distribution and severity of present soil erosion in New Zealand and referring to the New Zealand Land Resource Inventory (NRLRI) carried out between 1973 and 1979, Eyles (1983) defined sheet erosion as a process in which bare ground loses a thin layer of soil. Selby and Hodder (1993) call this type of erosion "wash erosion" and defines it as the detachment of soil by runoff, occurring where runoff is able to concentrate and the velocity of the flow reaches an erosive level. The velocity and the turbulences of the flow determine the size and the quantity of the transported grains, as well as the duration of the transport. Once in movement, only a decrease of the velocity can cause the deposition of the grains. Additionally, rain drops falling into overland flow water create splash and enhance entrainment (Selby and Hodder, 1993). Also an increase of the depth of the overland flow causes the soil transport rate to increase also.

Yang et al. (2006) used the environmental radionuclides ^{7}Be and ^{137}Cs as sediment tracers to estimate the relative contribution of sheet (interrill) and rill erosion to the total soil loss and their changes during an individual event. Carrying out surveys on two different erosion plots,

on a cultivated and on an uncultivated hillslope on the Loess Plateau in China, it was found that rill erosion is dominating the sediment mobilisation process.

Tunnel gully erosion

In the NZLRI tunnel-gully erosion was recorded where surface cave-ins, initiated by sub-surface tunnelling, or gullying resulting from these cave-ins, were observed (Eyles, 1983). Parker (1963) described the piping process leading to tunnel gullies in detail. A permeable, easily erodible layer on top of an impermeable layer, both cut by a gully wall or another free face, are needed. If, for example, due to a heavy rainstorm or over-irrigation the impermeable layer becomes saturated, the water seeps out of the face, carrying dispersed and disaggregated particles. In this manner a pipe is initiated which grows further into the bank, growing in diameter and creating new free faces for ground water discharge. Either the collapse of the roof of this channel, developing by this means, or the water and sediment flowing out of the free face can be the origin of a gullying process. Parker (1963) calls this process where subsurface flow develops to a gully 'piping'.

Bryan (2002) describes this process as a spontaneous development by outlet sapping, where the soil water potential is positive and particles are ejected or fabric macropores enlarged due to seepage forces produced by high hydraulic gradients. Accordingly, Selby and Hodder (1993) conclude that piping is found in many different types of climates and has its origin in soils that are saturated, which have a cracked surface, large and open macropores (sometimes with converging saturation flows), or where surficial flows are diverted. Bryan (2002) specifies these soils as saturated dispersed clays, loess, and organic soils. Parker (1963) defined the areas for piping occurrence as "areas where vegetation is sparse, thinning or denuded". Piping may develop on grassy soils where climate changes, overgrazing, etc. lead to plant cover reduction (Parker, 1963).

Diameters of pipes and tunnels can range from 2 cm up to more than one metre, their length from metres to kilometres, and the flow velocity in the pipes is comparable to overland flow velocities (Selby and Hodder, 1993). Various studies on the Loess Plateau in China in the middle reaches of the Yellow River showed that tunnel diameters can reach diameters of even up to 4.8 m (Zhu et al., 1997, 1999, and 2002).

Concerning gully erosion in particular – as a dominating and very obvious form of erosion on the foothills of Banks Peninsula, Poesen et al. (2003) underline the importance of gullies in

terms of their contribution to soil degradation and sediment production. According to their research, 10 to 94 % of the sediment detached through erosion is caused by water yields from gully erosion. Bradford and Priest (1980, as cited in Poesen et al., 2003, p. 101) explained that with decreasing influence of interrill or rill erosion (e.g. on grassland covered slopes), the contribution of gully erosion to the total sediment production rises.

The Soil Science Society of America (2001) defines gully erosion as the erosion process whereby runoff water accumulates and often recurs in narrow channels and, over short periods, removes the soil from this narrow area to considerable depths.

Additionally, Poesen et al. (2003) distinguish bank gullies, which develop wherever an earth bank is crossed by concentrated runoff. They state that bank gullies can rapidly be initiated through hydraulic erosion, piping (as explained above) and eventually mass movement processes at or below the soil. Once developed, by headcut migration bank gullies proceed into the soil surface of lower gradients on the bank shoulder and further into low-angled pediments, river or agricultural terraces (Poesen et al., 2002).

Importantly, gully erosion is identified as a threshold phenomenon (Poesen et al., 2003), occurring only when certain boundary conditions are exceeded with regard to: flow hydraulics (e.g. boundary flow stress), rainfall (e.g. intensity), topography (e.g. slope gradient), pedology (e.g. soil shear strength) or land use (e.g. land cover change combined with heavy rainfall). Rills, gullies, and river channels are often distinguished by their diameter. Nonetheless, the transition rill erosion – gully erosion – river channel erosion should be regarded as a continuum (Poesen et al., 2003).

Creep

Soil creep is the movement of unconsolidated materials near the surface of the earth in the absence of overland flow (Roering, 2004). According to Selby and Hodder (1993), predominantly three types of creep can be distinguished: (1) Due to gravity, freeze-thaw and wet-dry cycles, and rain splash, *creep of single particles* is induced. The creep distance depends on the gradient and the length of the slope, and is inversely related to the particle size. (2) Where no distinct failure planes are evident, *depth creep*, a very slow and continuous movement process, occurs. Thereby the overburden is transported as mass above a zone of deforming material. (3) *Soil creep* is a mostly invisible, slow movement of superficial soil or rock debris, which plays a central role in the development of hillslopes, and is the cause for

the convexity of hilltops and slopes (Selby and Hodder, 1993). It occurs in areas where variable climate causes a constant change of expansion and contraction due to freeze-thaw, wetting-drying and heating-cooling processes.

In order to characterize precisely the entire process of creeping, Heimsath et al. (2002) used natural quartz to determine grain movements. The quartz grains were used as labelled soil grains, of which the movement from the time elapsed since each grain last visited the soil surface was determined. These measurements were carried out using single-grain optical luminescence dating. Downslope flux was calculated from soil production by weathering at the soil base. Similar to the present study, Roering et al. (2002) used a primary tephra layer within loess deposits along an undissected hilltop, and its depth decrease in downslope direction, to model transport rates driven by creeping. Their results showed that a very important - if not the most important - type of soil creep is biologically induced creep – through tree throw, root dilation of soil, or burrowing organisms.

Mass movement erosion

Hillslope erosion is not always caused by overland flow or creep processes. The main process in the development of hillslopes, especially those of steep and mountainous regions, is mass wasting. Mass wasting is the downslope movement of soil or rock material under the influence of gravity without direct aid of other media, such as water, ice or air (Selby and Hodder, 1993). In the Andes, the Rocky Mountains, and the Japanese and New Zealand Alps, slope failure can be attributed to a combination of extreme relief, high tectonic, volcanic and seismic activity and corresponding geological and climatic conditions, often in connection with widespread changes in vegetation or land use (Selby and Hodder, 1993).

Dietrich et al. (1995) explain the different processes on steep and hilly landscapes. In steep, soil-mantled landscapes, debris flows can be generated by shallow landsliding which clear out low-order channels, depositing large quantities of sediment in higher-order channels. On landscapes of lesser gradient – especially on unglaciated, hilly, mostly soil-mantled areas where Horton overland flow is absent or rare and the underlying bedrock mechanically strong – diffusive transport processes, like the above discussed creeping, predominate on divergent hillslopes and tend to fill areas of convergence between short periods of erosion by gullying or landsliding (mass wasting). In these phases of evacuation, accumulated sediment is removed and bedrock eroded. As a consequence, soils on narrow ridges tend to be thin; and, correspondingly, thick in convergent areas (Dietrich et al., 1995). This is also described by

Reneaú and Dietrich (1991) who showed that in areas of convergent topography (such as hollows) sediment accumulates, as these areas act as local traps for a proportion of the colluvium transported downslope. Thresholds of stability may be exceeded during heavy rainfall events, leading to landslides or debris flows. Bedrock emerges either where the sediment stored in the hollows is evacuated, mostly by shallow landslides, or where curvature causes the soil production rate to be exceeded by divergent transport (Dietrich et al., 1995).

Reneau and Dietrich (1991) carried out a study in the southern Oregon Coast Range, and estimated local hillslope erosion rates averaged over long time periods, using dated colluvial deposits in hollows. For the calculations calibrated radiocarbon age and size of colluvial deposits were determined as well as the size of the contributing source area. At the same sites, calculations of exfoliation rates were carried out, in order to provide an additional measure of hillslope erosion.

In their study in northern California Dietrich et al. (1995) proposed a model for the prediction of the spatial variation in colluvial soil depth. The results were used to examine the dependency of slope stability on root strength and vertically varying saturated conductivity. The authors showed that soil thickness strongly affects slope stability as it influences the soil pore water pressure and the availability of soil moisture. In steep unchannelled valleys with thick colluvial deposits slope instability is most likely. Shallow soils (30 cm) are more stable, even with minor root cohesion. Shallow failures were proved to be initiated by erosion of the toe of the failing area, caused by channel head advance (Dietrich et al., 1995).

1.2.2 Quantifying soil erosion rates

1.2.2.1 The ^{137}Cs technique

History and background

In the last half century the use of natural and human-made radioisotopes to measure soil erosion and sedimentation has become more and more applied (Zapata et al., 2002). Fallout ^{137}Cs, as well as cosmogenic ^{7}Be and natural ^{210}Pb, are three of the radionuclides that can be used for this type of study. While their two-dimensional distribution can be used to make inferences with regard to short-term (> 30 days), and medium-term (~ 40-100 years) average soil-redistribution rates, their vertical distribution allows conclusions with respect to the chronology of sediment deposition (^{7}Be: weeks; ^{14}C: thousands of years) and bioturbation

processes. Concentrations of the radionuclides can also provide information on catchment erosion processes.

^{137}Cs is the most widely used radionuclide in the assessment of soil redistribution, due to its relatively long half-life (33.12 years; Zapata, 2003), the uncomplicated measurement method, the well defined interval of fallout input, and its affinity to fine particles (Ritchie and McHenry, 1990; Walling and Quine, 1993). Hence, it is not surprising that in 2001 already more than 2,500 citations concerning the use of this technique existed (Ritchie and Ritchie, 2001, as cited in Zapata, 2003, p. 5).

There are no natural sources for ^{137}Cs. This radionuclide is the product of global atmospheric nuclear-weapon tests from the 1950s to the 1970s. Due to those tests ^{137}Cs was emitted into the stratosphere and globally distributed. It fell to the earth surface by rainfall. ^{137}Cs fallout started in 1954 and reached its peak around 1963. Since then (in part attributable to the Nuclear Non-Proliferation Treaty (NPT) ratified on July 1, 1968) it declined to very low, often undetectable levels. As with the other radionuclides, ^{137}Cs is measured using gamma ray spectrometry.

Inputs of ^{137}Cs in the northern hemisphere have been higher than in the southern hemisphere, due to the higher number of atmospheric nuclear tests in the northern hemisphere (Zapata, 2003). Bacchi et al. (2003) and also a review of the corresponding literature about ^{137}Cs applications in Australia and New Zealand support this fact. Bacchi et al. (2003) state that the low areal activity, measured in different studies in Brazil (~ 300 Bq cm^{-2}), is the main restriction for the use of the ^{137}Cs technique in that region. In fact, the values of areal activity measured in the northern hemisphere are up to ten times higher ($\geq$ 3000 Bq cm^{-2}; Bacchi et al., 2003). Nonetheless, the advantages of the application of this method have been demonstrated by researchers all over the globe (e.g. Basher, 2000; Zapata, 2003; Li et al., 2003).

Assumptions

Being an indirect technique, the application of the ^{137}Cs method requires various assumptions concerning the behaviour of ^{137}Cs in the environment, and the relationship between soil loss and ^{137}Cs loss. Basher et al. (1995) provide a short summary of the existing literature concerning the assumptions as relevant to the application of the ^{137}Cs technique in New Zealand:

- The temporal limit for the erosion estimates in New Zealand, using the ^{137}Cs technique, is set by the year 1953, when the first significant fallout was registered (Matthews, 1989, as cited in Basher et al., 1995, p. 789).
- The distribution of the initial ^{137}Cs fallout deposition was uniform, and uneroded sites retain a characteristic amount of the radionuclide.
- The redistribution of the radionuclide before being attached to soil particles is negligible. Biological and chemical processes have no big influence on the redistribution of ^{137}Cs, being mainly dominated by physical processes of erosion and deposition, or tillage. The net impact of soil redistribution is represented by a deviation from the ^{137}Cs value at the undisturbed reference site.
- If a relationship between soil loss and gain and ^{137}Cs loss and gain can be expressed by means of a certain conversion model, spatial variation of ^{137}Cs allows rates of soil redistribution to be calculated.

Advantages

Basher (2000) and Zapata (2003) summarise the advantages of the ^{137}Cs technique as follows:

- Cultivated and uncultivated soils can be examined.
- By contemporary sampling, medium-term (30-50 years) erosion rates can be assessed.
- Only a single set of measurements needs to be made.
- The results are time average data and as such less influenced by extreme events.
- Individual point data can be interpolated to areal information.
- The study area is not significantly disturbed by the sampling method.
- The results are compatible with GIS, modelling, and geostatistics.
- The results reflect the integrated effect of landscape processes and land management.
- Erosion, deposition, and therefore net rates of sediment transport are measured.
- There are no major scale constraints (apart from no. of samples).
- It allows the quantification of effects of soil tillage and sheet erosion.
- The technique can be applied in fingerprinting suspended sediment sources and in estimating rates of over-bank floodplain accretion.
- It has the potential to be used as an environmental indicator to monitor rates of surface erosion in the future.

Limitations

Zapata (2003) summarizes the limitations of the ^{137}Cs technique as:

- Need for multidisciplinary team and specialised laboratories (costly analysis);
- requirements for quality assurance/control of low level gamma spectrometry measurements;
- limitation to sheet erosion and general surface lowering;
- indirect approach;
- selection of adequate conversion model;
- medium-term erosion rates – no possibility to take into account short-term influences;
- need for further standardisation for worldwide application.

Basher et al. (1995) highlight the limitation of the assumption that the original distribution of ^{137}Cs is uniform. Random variability in the initial distribution limits the robustness of erosion rates calculated by comparing individual sampling sites with the reference site.

A study carried out by Porto et al. (2003) in Calabria (southern Italy) primarily addressed the limitation of the ^{137}Cs technique in connection with the choice of the adequate conversion model. In order to convert ^{137}Cs measurements into erosion rates, various theoretical models can be used – for cultivated as well as for uncultivated soils. Porto et al. (2003) compared the results of two different conversion models for uncultivated soil with the direct measurements of sediment outputs in the reservoirs of two small catchments. The results showed that the estimates of the two models were reasonably consistent with the measurements. Nevertheless, their performance was shown to depend on the magnitude of the erosion rates. This study underlines the opinion of Basher (2000) who identifies the development of robust and accurate calibration procedures for the measurement conversion as the primary research need in connection with the ^{137}Cs technique.

Prediction of reference values

Independent of the fact that total ^{137}Cs inputs are a lot higher in the northern hemisphere (Zapata, 2003), various studies (e.g. Low and Edvarson, 1960; Davis, 1963; Lance et al., 1986; Arnalds et al., 1989, as cited in Basher, 2000, p. 224) found that ^{137}Cs atmospheric fallout is a linear function of rainfall within a given latitudinal range. Basher refers to Matthews (1989) who developed the following prediction model for reference values in relation to rainfall, using records of fallout deposition of ^{90}Sr and ^{137}Cs:

Fallout-Cs = 53.4 + 0.67*R

Fallout-Cs ... cumulative ^{137}Cs deposition to the end of 1990 [Bq m^{-2}];
R ... mean annual rainfall [mm]

Cumulative deposition after 1990, the year ^{137}Cs fallout ceased, can be calculated with this equation. Basher and Matthews (1993 and 2000, as cited in Basher, 2000, p. 225) tested the performance of the model for New Zealand and proved its general applicability. Using 22 sites with known history covering a rainfall range from ca 350 - ca 2800 mm annual rainfall, they adapted the model to local conditions, for more precise results. Their prediction model for ^{137}Cs areal activity in undisturbed soils is

Fallout-Cs = 149.5 + 0.51*R

Following Basher's explanations, either equation provides a useful tool for independently estimating reference values and verifying local measurements of the reference value, despite the fact that the predicted fallout-Cs tends to be slightly higher than the values measured in the soil. Additionally, in order to use these prediction equations, it is necessary to correct either the measured values or the predicted values for radioactive decay in order to work with the same base year, as significant decay will have occurred during the time period since the adjusted model was derived.

Application in New Zealand and worldwide

In New Zealand the ^{137}Cs technique has been applied in various studies investigating rates of surface erosion. Basher (2000) provides an overview of the different studies. Erosion rates have been estimated for cropland on the Canterbury Plains (South Island), Pukekohe, Ohakune, and Manawatu (North Island), showing that in areas of intensive vegetable production soil redistribution driven by surface erosion is very high. Soil loss due to wind erosion has been detected on these study sites for arable cropland, but also on grazed rangeland with depleted vegetation cover in Otago and the Mackenzie Basin (South Island). The author states that the use of ^{137}Cs has made significant contribution to quantifying rates of surface erosion in New Zealand, providing field-based data on erosion rates.

During the last five years further studies have used the ^{137}Cs technique to assess the influence of different types of land use on soil erosion (Basher et al. 2002, 2004; Quine et al., 2003).

Environment Canterbury (Cuff, 2006) has used the technique since 1997 in the context of the establishment of a network of soil erosion monitoring sites on arable land. However, so far no studies have used ^{137}Cs to quantify hillslope erosion under pasture.

As mentioned above, on a global level the ^{137}Cs technique has been applied in a large number of studies. Yang et al. (2006) agree with Zapata (2003) on the fact that measures to reduce soil erosion and associated land degradation are of great importance in the context of sustainable development and environmental protection. Not only is soil the primary source of life, directly and indirectly speaking, but also does a sound soil management concept prevent hazardous events caused by soil erosion. The ^{137}Cs technique is an effective and valuable tool for obtaining reliable quantitative data, in order to document magnitude and patterns of soil redistribution and provide the basis for the development of effective soil conservation and sediment control methods (Zapata, 2003; Yang et al., 2006).

Zapata (2003) presents the so-called Co-ordinated Research Projects (CRP), which was formulated by the International Atomic Energy Agency (IAEA) in April 1993 in Vienna, Austria. The objectives of the two component projects were: 1) the assessment of soil erosion through the use of ^{137}Cs and related techniques as a basis for soil conservation, sustainable production and environmental protection (Soil Erosion CRP), and 2) sedimentation assessment by environmental radionuclides and their application to soil conservation measures (Sedimentation CRP). In the latter, New Zealand acted as agreement holder among ten participants. The main output of these projects was firstly, the development of refined and standardised methods and protocols for the application of the ^{137}Cs technique (published as a handbook: Zapata, 2002), and secondly, a large amount of directly comparable data on soil distribution rates in a wide range of environments (North America, South America, Europe, Asia, Australasia).

Application on site

- First steps

Zapata et al. (2002) suggest that, before choosing an adequate site and considering a sampling design that leads to a meaningful result, it is important to undertake preliminary investigation. This includes gathering background information concerning the environmental and socio-economic context (literature, reports...), as well as identifying conditions and cultural practices that influence erosion and sedimentation processes. Following this, during the first field visit a reconnaissance sampling should be carried out in order to determine the ^{137}Cs

distribution in the area, and to establish if a suitable reference site exists. Another important aspect is the documentation of the landforms and soils. In the case of surfaces with significant plan curvature, introducing across-slope convergence and divergence of flow (Figure 1.1), the overall landform is best described by the use of slope gradient, plan and profile curvature, and total catchment area.

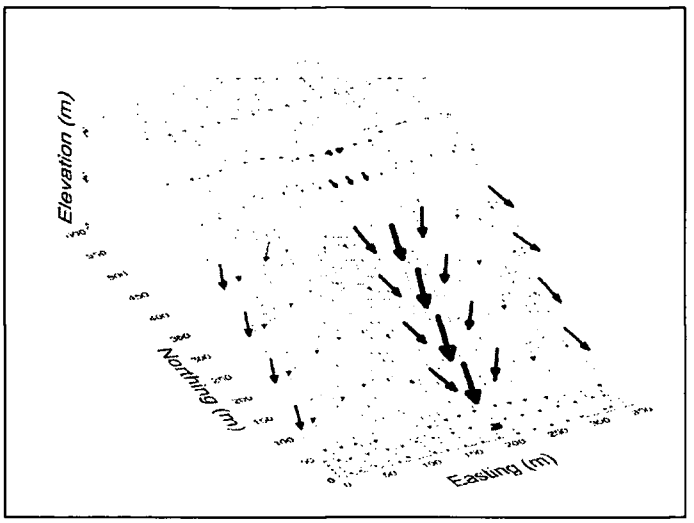

Figure 1.1: DEM of an undulating or dissected surface form (Source: Zapata, 2002).

- Site selection and sampling design

Pennock and Appleby (2002) list various principles to guide the selection of a reference site which will be used to assess the occurred movement processes at the real site of interest. These principles are:

- No upslope influences, no former soil loss or sediment deposition;
- continuous vegetation cover since begin of Cs-fallout – grass or low herb is best;
- close to sample site.

An important aspect in this context is the natural variability of the ^{137}Cs areal activity (Basher, 2000). Measurements of ^{137}Cs variability at sites throughout New Zealand as well as elsewhere in the world generally have coefficients of variation (CV) in the range 10-20 % (Sutherland, 1991 and 1996, as cited in Basher, 2000, p. 225). Basher (2000) underlines the importance of an exact characterisation of the natural variability of ^{137}Cs in the study area. He states that this is necessary to determine if locally measured reference values are based on adequate sample numbers, as well as for the interpretation of the ^{137}Cs measurements on the sample sites. He explains that to estimate the mean ^{137}Cs areal activity to ± 10 % at 90 % confidence interval, at most sites 10-15 samples are required.

Depending on the objectives of the specific research projects, the sampling design for the individual sample sites has to be chosen. For the assessment of erosion rates on different parts of a slope, for each element of the slope various core samples can be taken and mixed. Concerning the design of the sampling, Pennock and Appleby (2002) mention various approaches:

- *Haphazard sampling* is non-probability-based, using arbitrary selection of sample location. It is not recommended.
- *Judgement design* is non-probability-based too, but assumes that an experienced researcher, who has a good understanding of the system, is able to choose adequate sites, in order to demonstrate erosion processes.
- *Probability-based designs* are applied using systematic, non-stratified sampling, grids of different resolution (usually 10-25 m grid size), or using the systematic, but stratified grid approach where a grid is laid over the surface and the different points classified into the distinct types of slope (e.g. shoulder, backslope, footslope). Then, out of each class a number of points is chosen randomly, sampled, and the results for each class weighted by the proportion of the site it occupies.

Summarising, Pennock and Appleby (2002) propose the following guidelines:

- Systematic grid design for level reference sites;
- absence of significant plan curvature on simple slopes → one single transect (summit to toe);
- more complex slopes with significant curvature → non-stratified grid (summit to toe);
- complex slopes → systematic grid;
- geostatistical analysis → grid of two or more scales;
- analytical sampling → stratified grid.

o Sampling method

In order to quantify the depth distribution of fallout radionuclides, different devices have been developed. Depth-incremental sampling can be done, for example, using the "scraper-plate" method (an adjustable metal plate scrapes soil within a metal frame, e.g. 1 cm increments) or by using a router and a frame. Alternatives include cylindrical PVC core liners (Bacchi et al., 2000, as cited in Zapata, 2002, p. 47) – for soils with low cohesion, or the collection of intact

soil cores for distinct soil sections in soils with high cohesion. To determine the total inventory of ^{137}Cs at a single sampling point, one bulk sample taken from a soil core is collected and then analysed.

If in depositional areas sediments reach greater depths, the above mentioned methods are not adequate. Either they have to be modified or other approaches should be used:

- The use of soil augers is possible in cohesive soils and sediments. Depending on the auger, depth increments and surface area vary.
- The scraper method can be adjusted to greater depths by operating it from a pit that has to be dug aside of the original sample site.
- Also box-monolith cores are an alternative for determining variations in radionuclide contents, using a metal box to obtain soil-profile sections.

o Sample processing

The soil samples collected in the field should be dried, using air-drying or oven-drying procedures, depending on the volume of the sample (Pennock and Appleby, 2002). Then the samples are disaggregated, sieved and weighed. Bulk densities can be calculated using the known sample volumes. Finally the bulk density is multiplied with the specific activity (Bq kg^{-1}) to obtain the areal activity (Bq m^{-2}).

o Radionuclide measurement

^{137}Cs is measured by basic gamma spectrometry (Wallbrink et al., 2002). A widely applied technique is the use of high-resolution, low-level gamma spectrometry. In special detectors high-purity germanium interacts with the gamma photons emitted by the radionuclides which are contained in the soil. The detector emits signals in correspondence to the energies of the photons. Amplifying and multi-channel analysing the signals, their spectra can be converted into specific activities (Bq kg^{-1}) using calibration procedures.

o Calculation of erosion rate

The comparison of ^{137}Cs activities from the sample sites with the reference inventory enables the distinction between sites of net soil gains or losses, which then can be used to draw conclusions concerning the relationship between soil redistribution and topography, soil properties or land use (Figure 1.2).

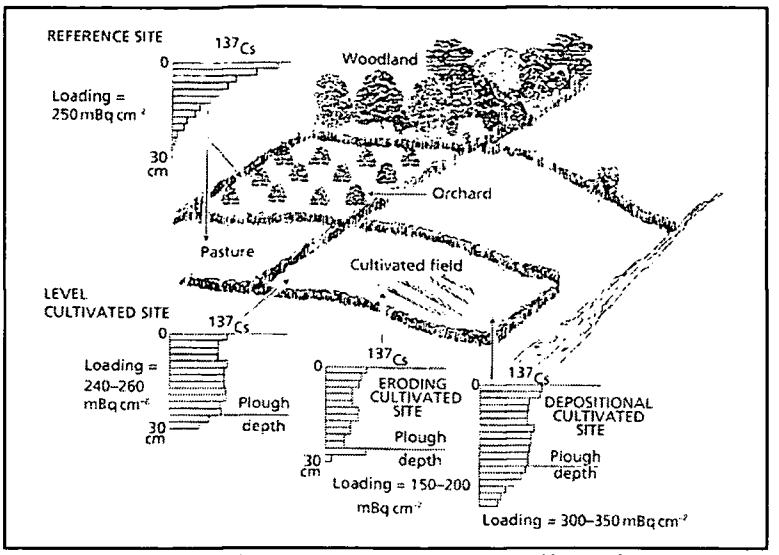

Figure 1.2: Schematic representation of the effect of erosion and deposition upon the loading and profile distribution of ^{137}Cs (Source: Morgan, 2005).

The outcome of these comparisons depends strongly on the quality of the applied conversion model – a mathematical relationship converting ^{137}Cs measurements into soil loss.

For undisturbed soils, in contrast to cultivated soils, Walling et al. (2002) distinguish between *profile distribution models* (the depth distribution is characterised by a numerical function) and *diffusion and migration models* (model of accumulation and vertical distribution of ^{137}Cs in the soil profile through time), with the latter being more precise but, as a consequence, more complex.

The *profile distribution models* and the *diffusion and migration models* are only two examples from a large number of calibration models. In order to choose the adequate approach for the particular investigation, distinguishing between cultivated and undisturbed soils, and weighing up simplicity versus accuracy are of great importance. Additionally, the availability of data may also be the limiting factor.

If the ^{137}Cs technique is to be applied on a site where cultivation is or was practiced, a model for cultivated soil has to be used. Following Walling et al. (2002) and Morgan (2005), the simplest and most widely used theoretical model for cultivated soil is the proportional approach, where the erosion rate depends on bulk density, depth of the cultivated layer, percentage reduction relative to the reference, and time.

1.2.2.2 Tephra tracer technique

Tephra – rock fragments and particles ejected by a volcanic eruption – establish isochronous horizons where their primary airfall deposit is preserved. In circumstances where a tephra layer of known age is buried and its relationship to a pre-existing landsurface is known, amounts and rates of erosion can be calculated. The change in concentration of the tephra layer in the soil profile, and the change in depth to the tephra layer with respect to the existing ground surface can be used to calculate long-term rates of soil erosion or sedimentation along hillslopes (Roering et al., 2004). The premises for this method are that: 1) the layer is detectable, 2) the quantity of the particles which form the layer is measurable, and 3) the particles themselves are resistant to chemical weathering; e.g. the tephra is conservative (Walther, 2006).

This project exploits the trace occurrences of a ca 26,500 year old volcanic ash in loess deposits that form the soils of Banks Peninsula. Similar studies carried out by Roering et al. (2002, 2004) described the use of a tephra layer within loess deposits in North Canterbury, New Zealand, in order to quantify rates of soil transport and investigate soil transport mechanisms in absence of overland flow. It was demonstrated that with increasing slope convexity, and consequently increasing gradient and landscape lowering rate, the depth to the tephra layer decreased (Figure 1.3).

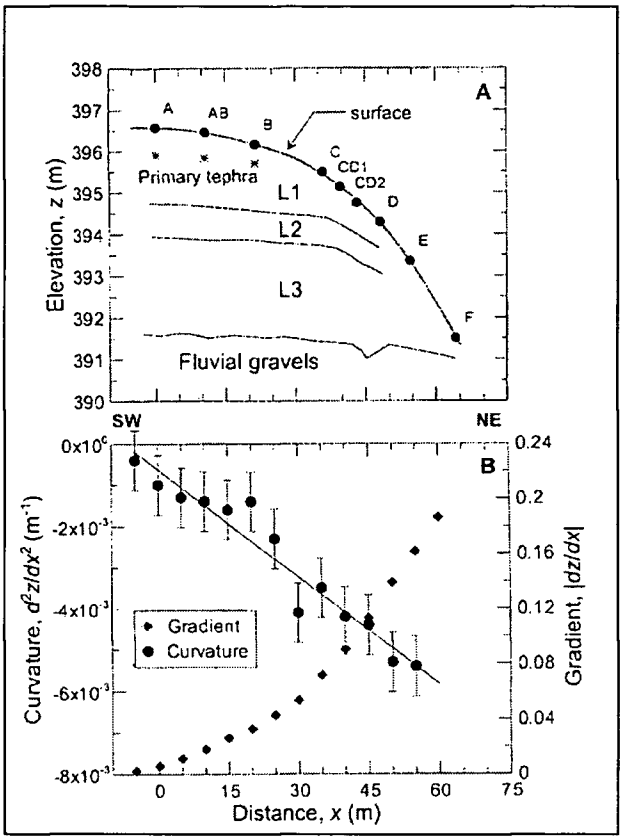

Figure 1.3: Relationship between slope length, curvature, elevation and tephra location (Source: Roering et al., 2002).

Additionally, it was shown that at a certain extent of tephra exhumation by erosion, the tephra became uniformly mixed in the upper, biologically active, 40-50 cm of soil. From the top of the slope to its foot, the tephra layer turned from thin and highly concentrated at depth into less concentrated and widely distributed in the upper soil. This pattern was interpreted as indicating soil creep transport processes driven by tree-related bioturbation, which include windthrow and root dilation of the soil, being the dominant soil mixing and transport mechanisms.

Similar patterns of tephra distribution were found on a forested hillslope in the Pacific Northwest of the USA. Walther (2006) used a tephra layer to investigate and quantify transport mechanisms and rates. She used two approaches to trace the processes acting on a hillslope and affecting the sediment transport. In the first, the tephra layer acted as a marker bed, with the change in depth to the concentration peak used to estimate erosion since the original deposition. In this case the assumptions made were that the peak was still visible, that the decline in depth to the primary tephra layer was only due to erosion, and that the active layer (upper soil layer, prone to disturbances by soil creep and biologic activity) was not necessarily well-mixed. In Walther's (2006) calculations it was also assumed that soil

transport effectively turned on ca 6000 years ago when forest 'returned', replacing a grassland landscape.

In the second approach the change of tephra concentration in downslope direction was assumed to reflect the amount of soil erosion. The assumptions were that the active soil layer was well-mixed, and that the original deposition is represented by the tephra inventory near the crest of the slope. This method is equivalent to the proportional approach used with ^{137}Cs. Walther applied a counting method similar to the one used in the study of Roering et al. (2002), and described in detail a so-called "spiking technique", a method comparable to those used in pollen analyses, which was developed by Dr. Peter Almond at Lincoln University, New Zealand (yet unpublished).

1.2.3 Slope stabilising properties of vegetation

Concerning erosion properties of loess-covered slopes with and without vegetation, a study of Rejman et al. (1998) on a small agricultural watershed of one of the largest loess belts of southeast Poland showed that soil properties of the plough layer were highly variable within short distances. The localization of soil erosion classes – depending on the primary differentiation in loess cover, intensity of erosion processes and agricultural activity in the past – could not be identified with the actual landscape position. Nonetheless, the results showed that soil losses registered on slightly and moderately eroded soils, were half as high as on severely eroded and colluvial sites.

Wainwright et al. (2000) carried out a series of rainfall-simulation experiments in the American South-west on soils developed on Quaternary alluvium, in order to observe changes in process and flux-rate resulting from the replacement of the dominant vegetation type from grassland to shrubland. Aside from variations in infiltration rates, flow hydraulics, splash and interrill erosion rates and nutrient transport rates, the results demonstrated that the shrubland areas develop rills, which are responsible for significant increases in overall erosion rates.

Xinxiao et al. (2006) describe a series of surveys carried out from 1982 to 2000 in the loess area of the Lüergou watershed, in China. The results of the analyses of observation data, climate data and aerial images, and the consequent multi-variable regression, showed that with increasing precipitation indices and decreasing plant coverage the amount of sediment production due to erosion increased significantly. However, the contribution ratio of changes in precipitation was even higher than that of the vegetation cover.

Pan et al. (2006) conducted laboratory-simulated rainfall experiments to investigate the runoff and sediment processes on sloped loess surfaces with and without grasses and moss coverage under different slope gradients. Interestingly, the average runoff rates and runoff coefficients on plots without grass were lower than on those with vegetation cover. Pan et al. (2006) attributed this behaviour to the reduction in water infiltration under moss. However, sediment yields from grass covered plots only came to 45-85 % of the rates from plots without coverage. In both cases sediment delivery reached steady state at a certain time. This behaviour was clearly different from that of the sediment delivery increase with rainfall time on bare sloped land under similar experimental conditions (Song et al., 2003), which mainly results from rill development on bare sloped land. Interestingly, this did not happen in the experiments of Pan et al. (2006).

Soil bioengineering is a subdiscipline of ecological engineering (Kangas, 2004), and aims to control soil erosion, combining civil or geotechnical engineering techniques with the use of vegetation plantings. For the stabilisation of slopes and the prevention of the detachment of soil particles various soil bioengineering measures have been developed, which utilise the stabilising properties of vegetation. Centuries ago, wood and plants were the only materials involved in the stabilising constructions. Today there is a trend back to these methods, whereby new and more extensive knowledge about the engineering properties of vegetation enables improvement of old methods or creation of new ones (Florineth, 2001).

Specialists in this area, for instance, Grey and Sotir (1996), Florineth and Rauch (2001), Schiechtl and Stern (2002), and Graf et al. (2003) have developed a large number of effective soil bioengineering methods. Nevertheless, it appears there is limited application of these measures to loess-mantled slopes, or study of the stabilizing effect of special types of vegetation on such terrain.

2 STUDY AREA AND STUDY SITE

2.1 Geographic location

The hillslope chosen for this project is located on the loess-covered foothills in the west of Banks Peninsula, in the surroundings of Taitapu, close to the Ahuriri Road and quarry in the South Island of New Zealand (Figure 2.1). Its coordinates (NZMG) are approximately 2476240 (Easting) and 5722740 (Northing) (GK: 43°42'07''S, 172°34'58''E).

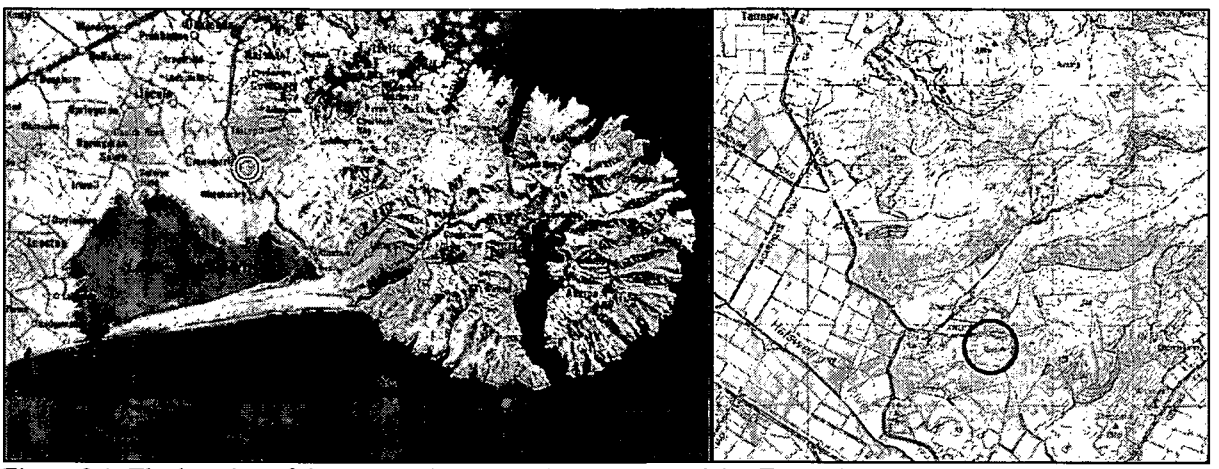

Figure 2.1: The location of the survey site near Taitapu (Source: Map Toaster).

2.2 Physiographic and geological setting

Banks Peninsula is situated on the eastern margin of the Canterbury Plains. It consists of two eroded extinct Miocene stratovolcanoes, Lyttelton in the northwest and Akaroa in the southeast, and some minor volcanic centres, and covers an area of approximately 1,200 km^2 (Sewell et al., 1993). The largely basaltic volcanic complex (Shulmeister et al., 1999) was originally an island which was connected to the Canterbury Plains by the outwash fans of the Waimakariri River in the Upper Pleistocene, approximately 20,000 years ago (Griffiths, 1973; Trangmar and Cutler, 1983). The peninsula has been heavily eroded, and along the outer flanks steep-sided valleys have been incised and/or exhumed. These valleys, which supposedly developed before the forming of the two calderas (Shelley, 1989, as cited in Shulmeister et al., 1999, p. 103), in combination with big gullies cut into the hillslopes, give Banks Peninsula the appearance of a largely dissected surface with a general radial drainage pattern. Thereby, the rather low gradients of the radially diverging ridges contrast with the steep walls of the valleys (Figure 2.2).

Figure 2.2: Aerial photo of Banks Peninsula illustrating radial drainage pattern and total and local reliefs (Source: Tufts University, 2006).

The whole peninsula was originally covered by a various metres thick loess-mantle, derived from the Waimakariri River, which transports sediment originating from the Southern Alps' greywackes. The aeolian sediment was translocated to the peninsula during periods of prevailing north-westerly winds (Griffiths, 1973; Shulmeister et al., 1999).

The data from the New Zealand Land Resource Inventory, carried out between 1973 and 1979, demonstrate – in concordance with the description of Griffiths (1974) – the prevalence of tunnel-gully erosion in the study area. On the South Island this type of erosion is typical for loess-covered rocks, and it is often associated with wash erosion (Eyles, 1983). Figure 2.3 shows the distribution of rock and erosion types on Banks Peninsula and the location of the study site.

A

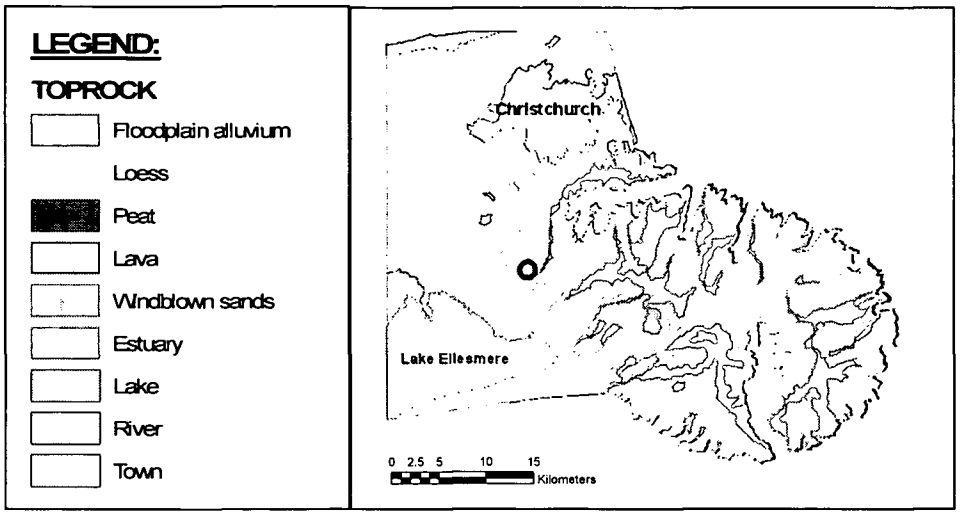

B

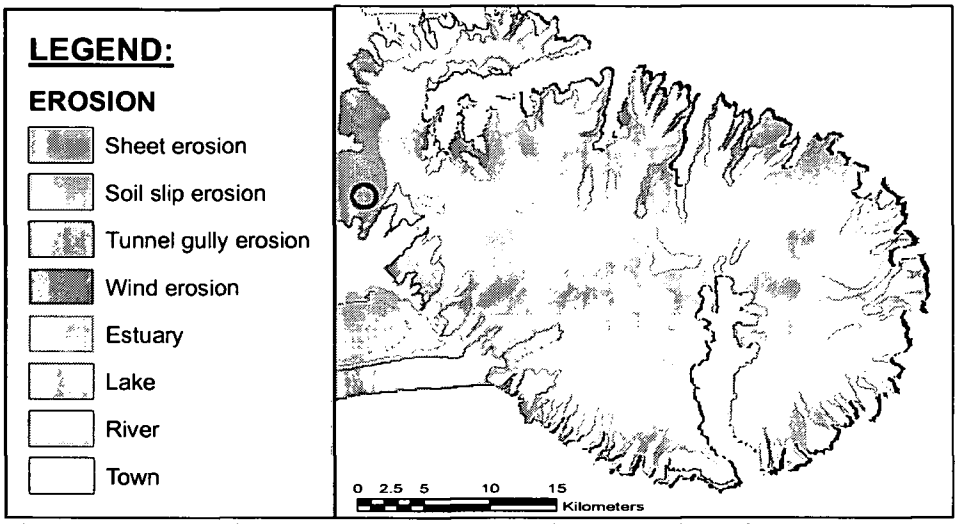

Figure 2.3: A: Rock type distribution on Banks Peninsula and B: Erosion type distribution on Banks Peninsula (Data source: NZLRI).

The tephra used for the determination of the long-term erosion rates is the same 26,500 cal yr BP (Wilson et al., 1988) (Kawakawa) tephra, originating from the Taupo volcanic zone, which was exploited by Roering et al. (2002, 2004). Figure 2.4 shows the areal distribution of the tephra.

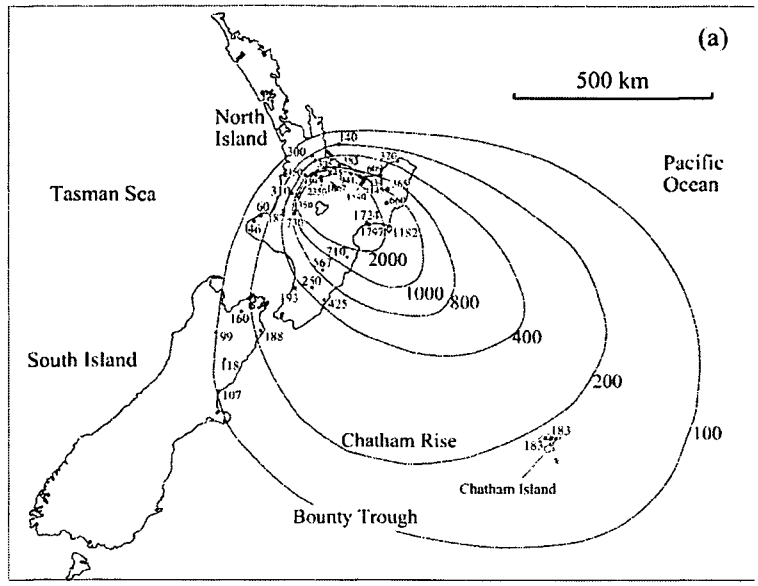

Figure 2.4: Isopachs of the Kawakawa tephra from Taupo volcanic zone [mm] (Source: Wilson, 2001).

2.3 Study site

2.3.1 Selection

The study site is a convex hillslope situated on a north aspect of a long ridge running in NE-SW direction from the summit of the Lyttelton volcano to the coastal plane adjacent to Lake Ellesmere (Figure 2.1). The hillslope transect studied was restricted to the upper convex slope segment from the interfluve to the upper backslope. This section of the slope is characterised by low profile curvature and limited micro-topography. This restriction has been made because the soil creep-type processes presumed to dominate here (Gilbert, 1909; Dietrich et al., 2003) satisfy the assumptions of the ^{137}Cs erosion measurement techniques employed. Below the upper backslope, tunnel-gully erosion predominates and soil erosion rate is likely to be highly spatially and temporally variable. Nonetheless, to test the influence of the gullies incising into the slope, the lower most of the sample sites was located on a spur between two gully heads. Figure 2.5 shows the location of the study transect in relation to the Ahuriri quarry.

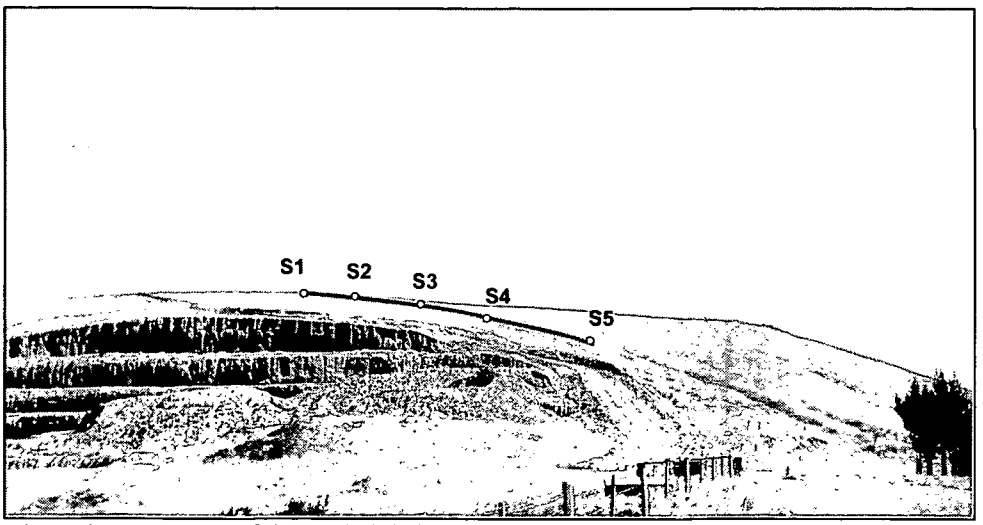

Figure 2.5: Location of the study hillslope.

A north aspect was chosen because slopes of this aspect receive higher insolation and are more exposed to desiccating north-westerly föhn winds than south facing slopes. They therefore were expected to be more prone to pasture dieback in summer, and hence have a greater propensity for rainsplash erosion than their southerly-aspect counterparts.

2.3.2 Soil pattern at the site

The slope is mantled with calcareous loess of the Birdlings Flat Formation, deposited in various layers (Griffiths, 1973). The soil formed on the loess in the whole Ahuriri area is loamy fine sand of the Takahe series (Griffiths, 1973); more specifically Takahe silt loam on the top of the ridge and Takahe hill soil on the slopes (Griffiths, 1974). Griffiths (1974) describes the different soils of the Takahe series in detail:

Takahe silt loam occurs on the rolling tops of spurs – as in the present study – and is developed on primary loess or loess colluvium. Depending on the location on a ridge, the depth of the topsoil ranges from 15-30 cm on the crests to 30-45 cm on the sides, and 60 cm at the toes where colluvial material has accumulated. Correspondingly, on the upper convex section of the slopes the topsoil is thinner, due to erosion.

At the nearby quarry the soil at the ridge crest, which had had the A-horizon removed, included the following horizons: B-horizon - Bw(f), 0-17 cm, silt loam; Bt(f), 17-30 cm, clay loam; Bx, 30-155 cm, silt loam to loamy fine sand; C-horizon - 2C, 155-188 cm, loamy fine sand; 3BCt, 188-197 cm, silt loam; 4C, 197-206 cm, loamy fine sand; 5C, 206-245 cm, loamy fine sand) (Shanhun, 2004; Appendix 4). Figure 2.6 shows the exposure of the adjacent soil at the Ahuriri quarry.

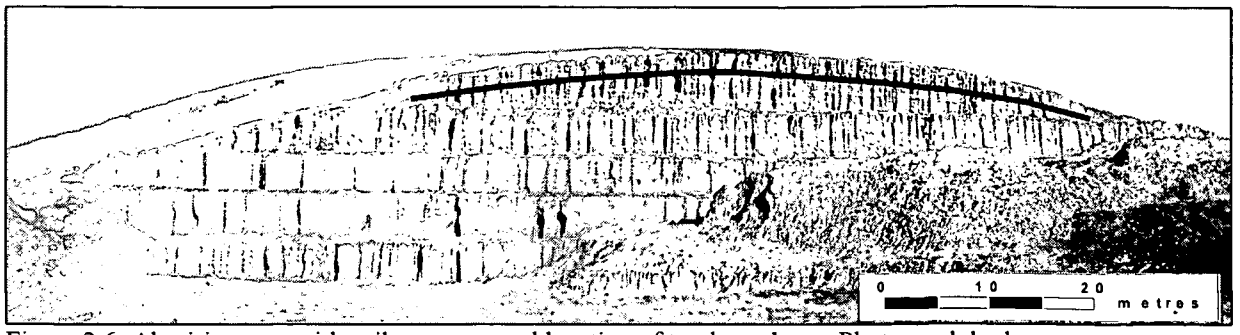

Figure 2.6: Ahuriri quarry with soil exposure and location of top loess layer. Photograph looks west.

2.3.3 Vegetation

Laing (1927, as cited in Griffiths, 1973, p. 653) reported that the native vegetation in the humid area had been bush and forest, and in the subhumid zone generally tussock. In contrast, Shulmeister et al. (1999) showed (from pollen analysis) that the original vegetation cover of large areas such as broadleaf forests was eliminated during glacial periods and replaced by tall shrubland. Enhanced by the alteration of the vegetation cover, the loess mantle was removed or re-deposited by movements induced by freeze-thaw processes in periglacial periods of the Pleistocene (Griffiths, 1973). Today, on the flank of the Banks Peninsula volcanoes the ridges are loess-mantled, whereas the valleys are filled with alluvium (Shulmeister, 1999).

The forest cover surviving the glacial elimination – podocarp and hardwood forest on the Port Hills of Banks Peninsula – was removed within the last thousand years by Polynesian, and later more intensively, by European settlers. Additionally, large areas have been covered with tussock for centuries. Further modification of the vegetation cover was brought about by clear cut, grazing, exotic forest plantings, urban sprawl, etc. (Wilson, 1992). The changes in vegetation cover were illustrated by Wilson (1998; Appendix 5). Today, the predominant tussock vegetation differs from the dense silver tussock met by the first European settlers, being further thinned out especially due to intertussock pasture (Wilson, 1992).

Situated on higher altitudes of the Ahuriri area the 'Ahuriri Bush' represents a very significant stand of bush on the Port Hills, consisting of extensive second-growth hardwood forest and areas of old-growth forest with abundant podocarps (Wilson, 1992). This type of forest may be representative of the Holocene vegetation at the study site despite the higher rainfall than at the Ahuriri Quarry.

2.3.4 Cultivation history

Consultation with the land owner revealed that in the last 20 years neither cultivation of any type nor sheep grazing have taken place. The only agricultural use of the hillslope has been as meadow for cattle. Additionally, the farmer conveyed his view that no severe erosion processes were going on, rather that the trampling by the cattle was "stabilising the ground".

2.3.5 Climate

According to the climate classification of Köppen (1931), New Zealand as a whole has a designation of Cfb (Robertson, 1956), that is a warm, temperate, rainy climate with no marked dry season. This climate type is characterised by temperatures of its coldest month between +18 °C and -3 °C, and of its warmest month higher than +10 °C. Köppen's system is, however, not sensitive enough to distinguish climatic districts within New Zealand (Robertson, 1956). Griffiths (1973) described the climate at high elevations of Banks Peninsula as humid (mean annual rainfall > 900 mm), and for lower elevations, as in case of the study site, as subhumid (650-900 mm) – except the eastern segments, where the climate at sea level is humid too. Long-term records of the land owner regarding annual rainfall resulted in a mean value of 690 mm yr^{-1}.

This climate regime commonly results in a summer soil moisture deficit, which leads to die-back of the pasture species and, as a consequence, exposure of the underlying soil. At these times the soil is susceptible to rainsplash erosion and possibly, in very intense rainstorms, overland flow erosion. By quantifying the erosion rate under the existing agricultural pasture and comparing it to the long-term erosion rate under the changing climate and vegetation regimes since the last glacial maximum, the importance of anthropogenic effects on the erosion rate can be assessed.

3 METHODS AND MATERIALS

3.1 General approach

Long- and short-term erosion rates for the study area were quantified as follows:

1) The hillslope transect was surveyed topographically at high resolution.
2) Five sites were sampled along the transect and analysed for ^{137}Cs and tephra distribution and concentration. ^{137}Cs reference sites (uneroded) were sampled on the interfluve.
3) Short-term and long-term erosion rates were calculated for each site, using ^{137}Cs profile inventory, tephra grain inventory, and depth to tephra emplacement horizon.
4) A slope dependent transport model was parameterised to encapsulate transport efficiency relevant to the short and long time scales, and the parameters used as a basis for comparing soil erosion rates at different time scales.

3.2 Slope morphometry and topographic analysis

In order to relate sites and the associated erosion rate estimates to local hillslope geometry, a high accuracy RTK GPS survey was conducted. The elevational (z) accuracy of this type of measurement lies in a range of ± 5-10 cm, the horizontal positioning accuracy within 1 cm. The size of the surveyed slope area is approximately 30x100 metres. In total 2,633 points were measured.

Slope curvature, necessary for the parameterisation of the transport model (see Section 3.5), was calculated by fitting a second-order polynomial, transformed to an origin at the sample sites, to the x, y, z coordinates adjacent to each sample site by least squares regression. The curvature is given by the second derivative of the following expression interpolating the hillslope surface:

$$z = A*x^2 + B*y^2 + C*x*y + D*x + E*y + F$$

Taking the first derivative with respect to x and y at a time gives:

$$\frac{\partial z}{\partial x} = 2Ax + Cy + D \quad \text{and} \quad \frac{\partial z}{\partial y} = 2By + Cx + E,$$

and the gradient at a site is

$$\nabla z = \sqrt{\left(\frac{\partial z}{\partial x}\right)^2 + \left(\frac{\partial z}{\partial y}\right)^2}.$$

The second derivatives with respect to x and y are:

$$\frac{\partial^2 z}{\partial x^2} = 2A \text{ and } \frac{\partial^2 z}{\partial y^2} = 2B,$$

and the curvature

$$\nabla^2 z = 2*(\mathrm{A}+\mathrm{B}).$$

Five second-order polynomials were derived for each sample site using topographic data occurring within radii of 2.5, 5, 7.5, 10, and 15 m of the sample sites (Appendix 1). This was done to test the spatial variability of the topographic parameters.

3.3 ^{137}Cs methodology

3.3.1 Site selection and sampling design

In the present study, following the principles of Pennock and Appleby (2002), eight samples on the flat-topped interfluve were taken to determine ^{137}Cs reference values. As for all other samples a bucket auger with diameter of 8.8 ± 0.3 cm was used to collect soil. Each reference site on the interfluve was sampled in 10 cm increments and two sets of four samples were bulked by increment depth interval. On the basis of the results of the activity-distribution analysis for the bulked increment depth intervals at the interfluve reference sites IF1-4, where the main peak in areal activity was in the 0-10 cm increment (see Section 4.2), for the reference sites IF5-8 the increments 0-10 cm and 10-40 cm were bulked and the areal activity was determined.

Five sites were then selected along a transect from interfluve to upper backslope, following the judgement-design approach. Thereby, attention was given to choose five sample sites along the slope that were representative of the different sections of the hillslope. Three sites were located in the upper part of the slope where local curvature – and, presumably, with it

erosion rates – increased. The fourth site was located further down the slope above a gully head at the upper backslope. In this section headward migration of tunnel gullies had produced a cross-slope crenulation in the form of small gullies and spurs. This location for site four was chosen in order to observe the influence of the gullies on the erosion process. The fifth and lowest site was on the crest of one of the spurs. As mentioned above, tunnel-gully erosion is predominating below the upper backslope and, consequently, soil erosion rate is likely to be highly spatially variable. Hence, no sample site was selected in this section of the slope.

At the sample sites along the transect four auger holes were located within 1 m radius and sampled in 10 cm increments to 40 cm depth. Similar to the reference sites IF5-8, based on the results at the reference sites IF1-4, the top 10 cm increments of the borings were bulked for ^{137}Cs analysis, as were the 10-40 cm increments.

3.3.2 Sample preparation and analysis

The following steps of processing the ^{137}Cs samples obtained in the field were executed in accord with the procedure outlined by Pennock and Appleby (2002): The samples were air-dried and weighed. A bulk density was calculated using air-dry sample mass and increment sample volume (610 ± 40 cm^3). The ^{137}Cs samples were then ground and passed through a 0.5 mm sieve. Afterwards a ca 0.5 kg subsample was taken. This quantity is required for an accurate determination of ^{137}Cs activity. Activity analyses were carried out at the National Radiation Laboratory, Christchurch. Finally, to obtain the areal activity (Bq m^{-2}), the bulk density was multiplied with the specific activity (Bq kg^{-1}).

3.3.3 Calculation of erosion rate

As the study area is located on a hillslope without any cultivation during the last decades, the *profile distribution model* was used, as its accuracy has proved to be sufficient in similar studies (e.g. Li et al., 2003; Porto et al., 2003).

The erosion rate is calculated as follows:

$$Y = \frac{-10}{t-1963} * \ln(\frac{1-X}{100}) * h_0$$

Y ... erosion rate [t ha^{-1} yr^{-1}]

t ... year of sample collection [yr]

X ... percentage reduction in reference inventory (e.g. $(A_{ref}-A_u/A_{ref})*100$)

A_{ref} ... local reference inventory [Bq m^{-2}]

A_u ... measured total ^{137}Cs inventory at the sampling point [Bq m^{-2}]

h_0 ... coefficient describing profile shape [kg m^{-2}]; penetration depth of ^{137}Cs into soil

The factor h_0 was derived by fitting the following exponential function to the ^{137}Cs profile from one set at four bulked reference sites (Walling and He, 1997; Porto et al., 2001, as cited in Porto et al., 2003, pp. 399-400):

$$A(\chi) = A(0)*e^{-\chi/ho}$$

χ ... mass depth from soil surface [kg m^{-2}]

$A(\chi)$ ... concentration of ^{137}Cs at depth χ [Bq kg^{-1}]

A(0) ... concentration of ^{137}Cs in the surface soil [Bq kg^{-1}]

3.4 Tephra methodology

3.4.1 Site selection and sampling design

Adjacent to each of the five sites used for ^{137}Cs determination one hole was augered to at least two metres depth and sampled in 10 cm increments.

3.4.2 Sample preparation

Samples were air-dried, weighed, and a bulk density calculated, using air-dry sample mass and increment sample volume (610 ± 40 cm^3). The dry samples were sub-sampled to amounts of ~ 100 g as follows. The sample was divided into four quarters, and each quarter again subdivided into four even portions of approximately 25 g. By mixing only one portion of each quarter of the original sample subsampling effects should have been minimised.

3.4.3 Sample analysis

In order to be able to count the glass grains contained in the sub-samples, first they had to be cleaned. After removing the organic matter with H_2O_2 and heating the samples to about 100°C, the organic-free material was treated as follows, to remove iron oxides that aggregate and colour samples:

- Add 40 ml of 0.3M sodium citrate and 10 ml of 1M sodium bicarbonate.
- Heat to 80°C.
- Add 1 g sodium dithionite, adding ⅓ g at a time.
- Heat for 15 minutes.
- Sieve to 63 μm. The < 63 μm can be discarded.
- Wash > 63 μm fraction onto a labelled filter paper, dry at 60°C, and weigh.
- Transfer to clean, labelled vial.

The samples were then spiked with spherical glass beads at a concentration of 5 % w/w, to allow tephra grain concentrations to be calculated. The glass grains used (Potters Ballotini® Impact Bead, silica abrasion beads) range in size between 90 μm and 150 μm and are quoted by the manufacturer as having 664.8 x 10^6 grains/kg. The level of spiking ensured that the prepared samples had approximately 0.018 grams of beads per gram of sample.

The counting of the tephra involved sprinkling a small amount of sample (approximately 0.00334 g) into the well of a microscope slide and then immersing it in clove oil. The level of spiking was chosen in order to aim for about 40 spike beads per typical sample mass. Earlier work (Ducey, 2001) had shown this to be an optimal concentration for reducing counting effort while minimising glass count variance. The concentration of the tephra in the sample in increment was calculated as follows:

$$|T| = \frac{T}{S} * |S| * \frac{M_{>63}}{M}$$

$|T|$ ... concentration of tephra [grains/g]

T ... tephra grain counts

S ... spike grain counts

$|S|$ ... spike concentration in > 63 μm fraction [grains/g]

$M_{>63}$ ... mass of > 63 μm fraction [g]

M ... mass of subsample before cleaning and sieving [g]

The (isochronous) tephra emplacement horizon was identified by the peak in the distribution of the tephra along the profile. The thickness of soil above the emplacement horizon was used to determine the amount of erosion, as elaborated below.

3.4.4 Calculation of erosion rate

For the calculation of long-term erosion rates the assumptions made are that the tephra established an isochronous horizon in the landscape 26,500 years ago and that the deposition rate of the loess cover above the tephra layer originally was spatially uniform. These assumptions are reasonable because 1) loess is a suspension deposit that generally forms a mantle of uniform thickness at the local scale and is free of aeolian bedforms such as dunes that are associated with saltated deposits; 2) the hillslope having North aspect faces prevailing westerly winds and no lee/stoss side effects are expected; and 3) the exposure in the nearby quarry shows conformable layering at subunits within the loess and at least near the ridge crest a uniform thickness of subunits (Figure 2.6). Hence, the total amount of erosion can be calculated from the difference in depth to primary emplacement horizon, between sloping sites and interfluve site. The rate of erosion is determined by the difference in depth of original deposited loess and actual local loess coverage divided by the time since the tephra deposition. The following equations and Figure 3.1 illustrate this approach.

$$h_{net} = L - \Delta z$$

$$\Delta z = L - h_{net}$$

$$E = \frac{L - h_{net}}{26{,}500\,yr} \qquad (1)$$

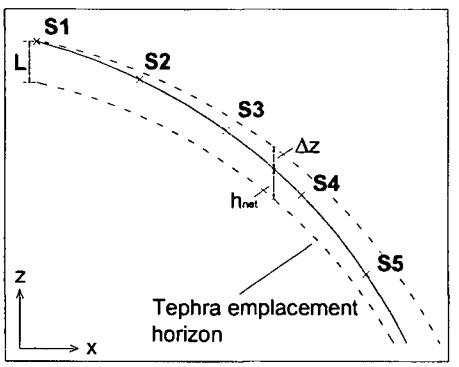

Figure 3.1: Schematic illustration of loess-covered tephra layer.

h_{net} ... net deposition

L ... total loess deposition as presented by thickness of loess above the tephra on the interfluve

Δz ... amount of erosion

E ... erosion rate

3.5 Modelling soil transport and erosion rate

The convex form of soil-mantled hillslopes results from slope dependent soil transport, modelled one-dimensionally as

$$\tilde{q}_s = -K * \frac{\partial z}{\partial x} \qquad (2)$$

$\tilde{q}_s$ ... sediment flux [$m^3\ m^{-1}\ yr^{-1}$]

K ... transport rate constant [$m^2\ yr^{-1}$]

$\frac{\partial z}{\partial x}$ ... local hillslope gradient

z ... elevation [m]

x ... horizontal distance [m]

The one-dimensional form of the equation is used for clarity. The argument can be extended simply to the two-dimensional case.

As sediment flux on steep slopes tends to increase nonlinearly (Roering et al., 1999), this model is appropriate only for low-gradient (< 0.4) hillslopes (Roering et al., 2002). Combining equation (2) with the one-dimensional continuity equation gives,

$$E = \frac{\partial z}{\partial t} = \frac{\partial \widetilde{q}_s}{\partial x}, \tag{3}$$

where,

E ... erosion rate [m yr^{-1}]

z ... elevation [m]

t ... time [yr]

$\widetilde{q}_s$ ... sediment flux [m^3 m^{-1} yr^{-1}]

x ... horizontal distance [m],

and consequently

$$\frac{\partial z}{\partial t} = K * \frac{\partial^2 z}{\partial x^2} \tag{4}$$

z ... elevation [m]

t ... time [yr]

K ... transport rate constant [m^2 yr^{-1}]

$\frac{\partial^2 z}{\partial x^2}$ ... local hillslope curvature

From equation (4) it is clear that the erosion rate $\partial z/\partial t$ is directly proportional to the local hillslope curvature, whereby K is a constant of proportionality, the transport coefficient. This

coefficient captures the efficiency of soil erosion, or the power of transport processes acting on the slope. A change in this parameter over different time scales is, therefore, a reflection of changes in intensity of erosion, as long as the slope dependent transport model is appropriate.

K can be estimated from the slope of a best fit line to a plot of erosion rate versus local hillslope curvature, or alternatively multiple values of K can be estimated from differences in erosion rates and curvatures from pairs of sites:

$$\Delta E_{ij} = K * \Delta C_{ij} \tag{5}$$

and

$$K = \frac{\Delta E_{ij}}{\Delta C_{ij}} \tag{6}$$

ΔE_{ij} ... difference in erosion rate between sites i and j [m yr^{-1}]
ΔC_{ij} ... difference in curvature between sites i and j [m^{-1}]

Over the long time scale and in the context of the hillslope studied, the model needs some modification since erosion and loess accumulation were happening simultaneously over some period after the deposition of Kawakawa tephra. In this situation the erosion rate is

$$\frac{\partial z}{\partial t} = \frac{\partial \tilde{q}_s}{\partial x} + l(t) = K * \frac{\partial^2 z}{\partial x^2} + l(t) \tag{7}$$

$l(t)$ ... time dependent loess accumulation rate [m]

The change in land surface elevation over the 26,500 years since the deposition of the tephra at a given location is given by,

$$\int dz = K * \frac{\partial^2 z}{\partial x^2} * \int_{-26.500}^{0} dt + \int_{-26.500}^{0} l(t) dt, \tag{8}$$

assuming slope curvature does not change significantly over the period 26,500 cal yr BP to present.

The second term on the right hand side of equation (8) is the total depth of loess that accumulated, here assumed to be the depth of loess, L, on the interfluve (Figure 3.1), and therefore,

$$\Delta z = K * \frac{\partial^2 z}{\partial x^2} * 26{,}500 + L. \qquad (9)$$

But Δz is equivalent to h, the thickness of soil above the Kawakawa tephra, and therefore,

$$h = K * \frac{\partial^2 z}{\partial x^2} * 26{,}500 + L. \qquad (10)$$

Assuming that the deposition rate of the loess cover above the tephra layer was relatively uniform at the sites along the transect as discussed above, the difference in soil depth above the tephra between two sites i and j then is

$$h_i - h_j = K * \left.\frac{\partial^2 z}{\partial x^2}\right|_i * 26{,}500 + L - K * \left.\frac{\partial^2 z}{\partial x^2}\right|_j * 26{,}500 - L, \qquad (11)$$

and similar to equation (5) and (6)

$$\Delta h_{ij} = K * \Delta C_{ij} * 26{,}500, \qquad (12)$$

and

$$K = \Delta h_{ij}/(\Delta C_{ij} * 26{,}500) \qquad (13)$$

Δh_{ij} ... difference in thickness of soil above Kawakawa tephra [m]
ΔC_{ij} ... difference in curvature at two sites i and j [m^{-1}].

Equations (10) and (13) reveal, similar to the statement above, that K can be estimated from the slope of a best fit line to a plot of erosion rate versus local hillslope curvature, or alternatively as the average value of multiple values of K, estimated from differences in erosion rates and curvatures from pairs of sites.

Departures from the linear relationship between differences in depth of soil above Kawakawa tephra and curvature would indicate an inappropriate model. Consequently, the assumption of a slope-dependent transport can be tested. A departure from a linear relationship would indicate transport process dependent on slope position, wind or overland flow erosion.

4 RESULTS

4.1 Hillslope morphology

The analysis of the topographic data of the studied hillslope showed an increase in gradient from ~ 2 % at the interfluve to ~ 35 % at study site S5 (Figure 4.1 and Table 4.1). This is still below the 'boundary' of 40 %, above which sediment flux tends to increase non-linearly (Roering et al., 1999) and the linear, slope-dependent transport model would not be appropriate (Roering, 2002).

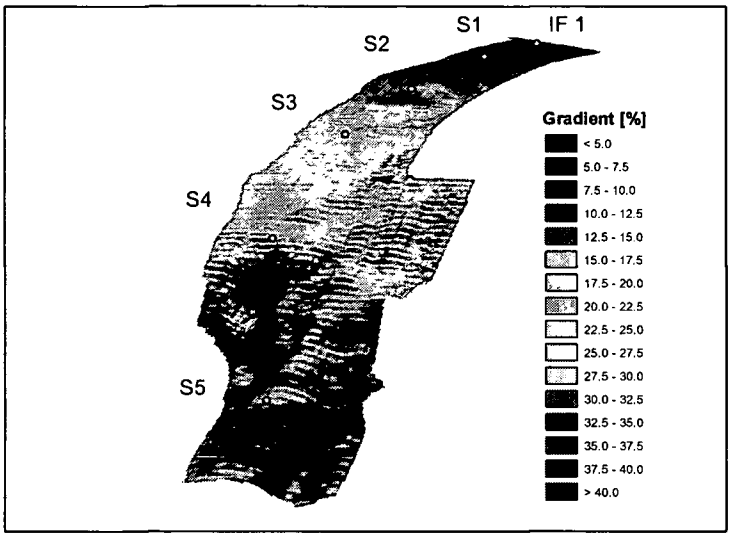

Figure 4.1: 3-D illustration of the hillslope and the sample locations. Shading indicates level of gradient.

At each sample site a set of five second-order polynomials was fitted by least squares regression, using the programme Genstat 8.2, to x, y, z data derived from the GPS survey from within 2.5 m, 5 m, 10 m, and 15 m radii (Appendix 1). Gradient and curvature were calculated (as the first and second derivatives of the polynomials, respectively; see Section 3.2) for each of the five polynomials. This was done in order to characterise the spatial dependence of these parameters, especially of curvature, and to determine the most appropriate value for each site (Figure 4.2).

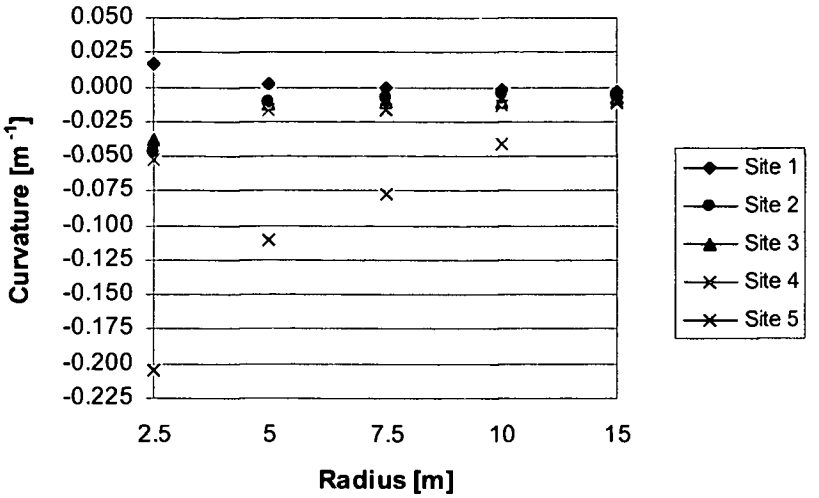

Figure 4.2: Total (plan plus profile) curvature values calculated for different radii of influence.

Curvatures for all sites except site S1 tended to decrease in convexity (curvatures become less negative) from small to large radii. At site S1 curvature at 2.5 m radius was positive (concave) but became planar by about 5 m radius and negative (convex) beyond 10 m radius.

For all sites except site S5 the curvature was accepted as being the average of the values forming a plateau in the respective curvature vs. radii plots. At site S5, however, the local micro-topography of spurs and gullies occurred over a spatial scale < 5 m, so that the 2.5 m radius was deemed most appropriate. At this site convex plan curvature contributed a large proportion of total curvature (Table 4.1, Figure 4.3).

Table 4.1: Elevation [m], Gradient [m/m] and curvature [m^{-1}] values at study sites

	Elevation	Gradient	±	Profile Curvature	±	Plan Curvature	±	Total Curvature	±
S1	73.01	0.0216	0.0006	-0.0023	0.0001	-0.0008	0.0002	-0.0031	0.0003
S2	72.18	0.0818	0.0008	-0.0037	0.0002	-0.0028	0.0003	-0.0065	0.0005
S3	71.07	0.133	0.001	-0.0085	0.0006	-0.0027	0.0008	-0.011	0.001
S4	66.28	0.256	0.002	-0.0115	0.0009	-0.003	0.001	-0.015	0.002
S5	59.53	0.35	0.01	-0.10	0.02	-0.10	0.02	-0.21	0.04

A

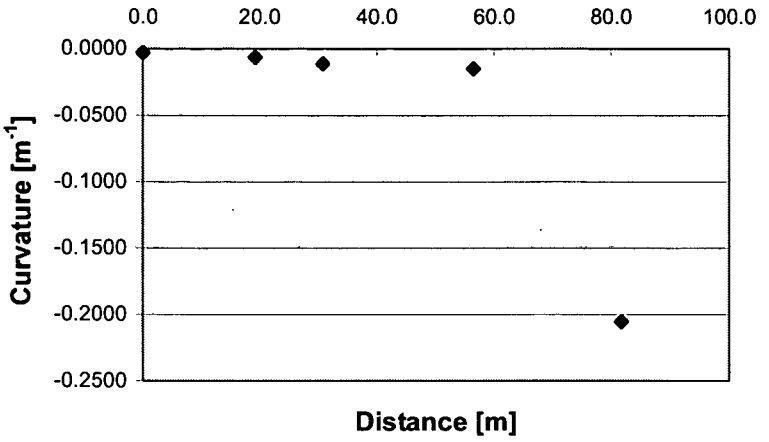

B

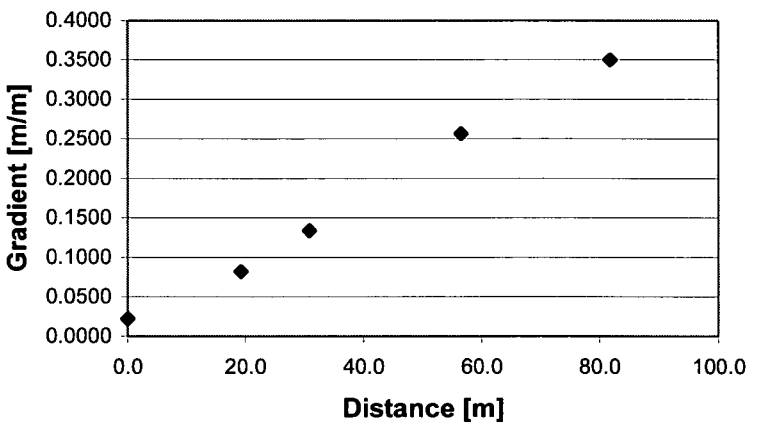

Figure 4.3: A: Total curvature and B: gradient at sampled sites along the transect.

4.2 ^{137}Cs reference value and depth profile distribution

Using the ^{137}Cs technique the net impact of soil redistribution is represented by a deviation from the ^{137}Cs value at an undisturbed reference site. Two determinations of a reference value made from flat interfluve sites (IF1-4 and IF5-8) produced similar areal activities, taking into account uncertainties, with an average of 343 Bq m^{-2}. Any real difference between the values at these two sites will be a result of the well documented spatial variability of ^{137}Cs deposition.

Using an estimate of 690 mm MAR for the study site, the predicted areal activity according to Basher and Matthews (2000, as cited in Basher, 2000, p. 225), corrected for decay over the period 2000 to 2006, is ~ 440 ± 10 Bq m^{-2}. Although the average values measured at the study

sites on the interfluve deviate from the predicted activities, especially at IF5-8 (306 ± 68 Bq m^{-2}, Table 4.2), these deviations are probably not significant given the fact that the model tends to overestimate activity values (Basher, 2000) and also taking into account the large uncertainty. Hence, the results of the activity measurements for the reference sites can be considered as within the range of the predicted values.

Table 4.2: Areal activity at reference and hillslope transect sites

IF 1-4	Sample Mass [kg]	^{137}Cs [Bq kg^{-1}]	± (2σ)	Areal Act. [Bq m^{-2}]*	± (2σ)
0 - 10	1.48	3.12	0.37	189	22
10 - 20	2.15	0.60	0.18	53	16
20 - 30	2.94	0.65	0.20	79	24
30 - 40	3.81	0.39	0.16	61	25
	Total: 10.38		Total Act.:	382	87
IF 5-8					
0 - 10	2.03	3.25	0.39	271	33
10 - 40	8.71	0.29	0.29	35	35
	Total: 10.74		Total Act.:	306	68
S1					
0 - 10	1.93	3.31	0.56	263	44
10 - 40	10.50	0.58	0.21	83	30
	Total: 12.43		Total Act.:	346	74
S2					
0 - 10	1.82	3.74	0.62	280	46
10 - 40	10.31	0.34	0.34	48	48
	Total: 12.13		Total Act.:	328	94
S3					
0 - 10	2.01	3.15	0.54	260	45
10 - 40	10.41	0.78	0.24	111	34
	Total: 12.42		Total Act.:	371	79
S4					
0 - 10	2.78	1.84	0.38	210	43
10 - 40	10.83	0.32	0.32	47	47
	Total: 13.61		Total Act.:	257	90
S5					
0 - 10	2.88	2.12	0.39	251	46
10 - 40	11.84	0.32	0.32	52	52
	Total: 14.72		Total Act.:	303	98

* areal activity = sample mass x activity/surface area of auger core

In order to calculate the magnitude of soil loss or gain on the basis of ^{137}Cs inventory, it is necessary, using the profile distribution conversion model (Chapter 3), to characterise the shape of the areal activity distribution of a profile and as such the penetration depth of ^{137}Cs into the soil. This is achieved by assuming an exponential depth distribution and determining the shape parameter h_0. Site IF1-4 was sampled at 10 cm increments for this purpose (Figure 4.4).

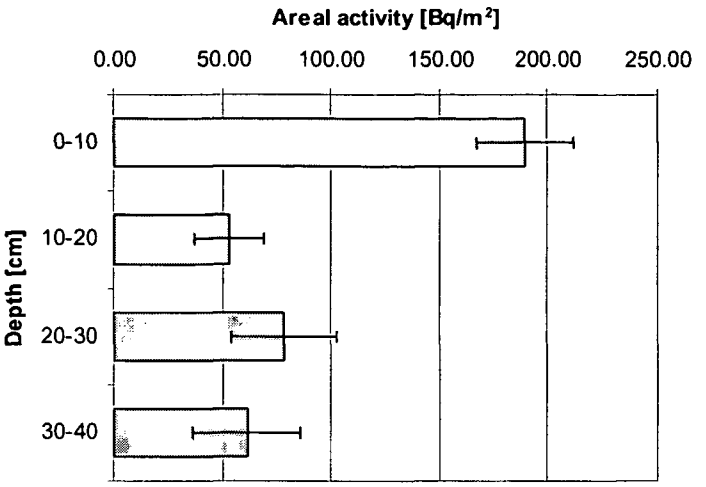

Figure 4.4: Areal activity distribution at reference site IF1-4

To determine h_0, mass depth χ is plotted against the natural logarithm of (1-cum.A_χ/A_{ref}) (cum.A_χ [Bq m^{-2}]... cumulative areal activity of ^{137}Cs at mass depth χ [kg m^{-2}]; A_{ref} ... total areal activity of ^{137}Cs of the soil [Bq m^{-2}]) and the coefficient derived as the reciprocal value of the slope of the regression line fitted to the resulting graph (Table 4.3, Table 4.4, Figure 4.5, and Appendix 6).

Table 4.3: Data and variables for deriving the ^{137}Cs profile distribution shape parameter h_0

Depth Increment	Depth	Bulk Density	Mass Depth	^{137}Cs Conc.	^{137}Cs Areal Act.	cum.A_X	1-cum.A_X/A_{ref}	ln(1-cum.A_X/A_{ref})
[cm]	[cm]	ρ [g cm^{-3}]	X [kg m^{-2}]	[Bq kg^{-1}]	A_X [Bq m^{-2}]	[Bq m^{-2}]	[-]	[-]
0 - 10	5	0.61	30.4	3.12	189.4	189.4	0.50	-0.68
10 - 20	15	0.89	105.0	0.60	53.1	242.5	0.37	-1.01
20 - 30	25	1.21	209.7	0.65	78.5	321.0	0.16	-1.83
30 - 40	25	1.57	348.4	0.39	61.1	382.2	0.00	
					A_{ref}:	382.2		

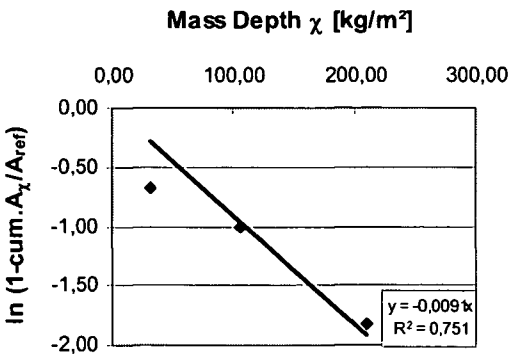

Figure 4.5: Derivation of h_0 as reciprocal value of regression line slope.

Table 4.4: Regression results for h_0 determination

Coefficient s	Standard Error	$h_0 = -1/s$	±
0.009	0.001	109	15

The resulting value of $h_0 = 109 \pm 15$ is similar to the value of the shape parameter reported in other studies (e.g. Li et al., 2003; Porto et al., 2003).

4.3 Hillslope ^{137}Cs distribution, erosion rates, and short-term transport parameter K_{short}

On the basis of the shape of the depth profile at reference site IF1-4, in order to reduce sample numbers and costs, for the reference sites IF5-8, and for the five transect sample sites S1 to S5, the increments 0-10 cm and 10-40 cm were bulked and the areal activity was determined (Table 4.2) (compare Section 3.3.1). For better comparability with other sites, in Figure 4.6 the activity values for the 10-40 cm interval of sites IF1-4 have been combined.

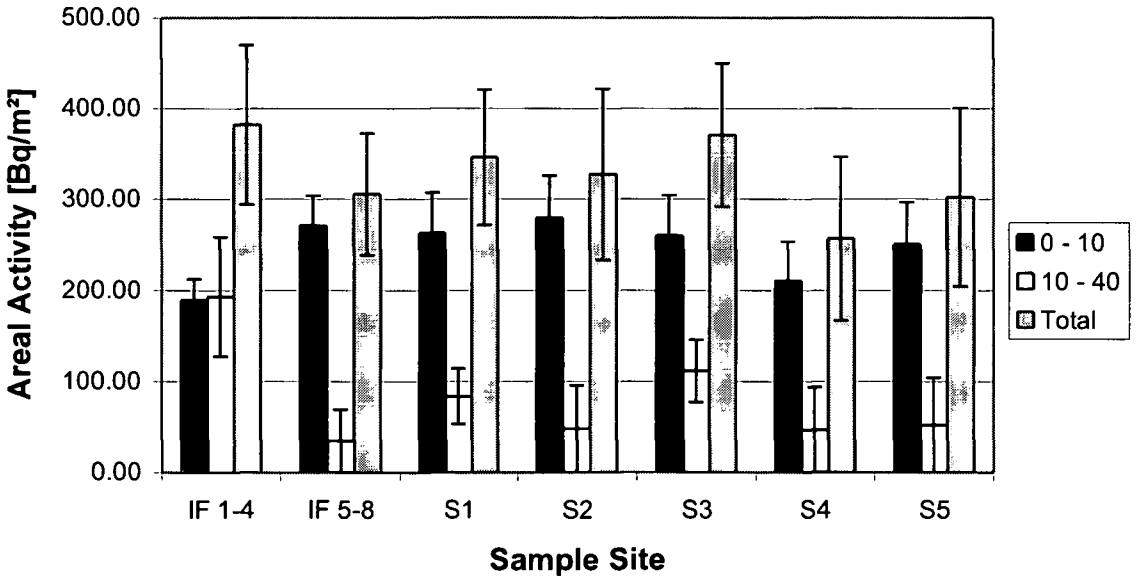

Figure 4.6: Areal activity distribution for reference and hillslope transect sites.

Taking uncertainties into account, the total areal activities of all sites, except perhaps S4, are indistinguishable, indicating that erosion during the last ca 50 years has not been significant enough for it to be detectable above the noise of the measurement errors and spatial variability. The distributions of ^{137}Cs between sample increments (0-10 cm and 10-40 cm) are also very similar among sites, the exception being site IF1-4. The difference for the latter site is, however, probably attributable to the imprecise depth sampling imposed by the auger sampling technique employed. The IF1-4 0-10 cm sample appears to be a thinner increment

containing ^{137}Cs-enriched surface soil undiluted by less ^{137}Cs-rich soil from below. This explanation is supported by the relatively low total sample mass of the IF1-4 0-10 cm increment (Table 4.2) and by the anomalously high ^{137}Cs concentration in the IF1-4 10-40 cm increment. This deeper increment has probably captured some ^{137}Cs-rich surface soil that the deeper increments at the other samples sites have not.

The trend of increasing total sample mass with distance downslope (compare Table 4.2) is indicative of erosion rate increasing downslope, lowering the A horizon of the soil more rapidly into the dense subsoil. The differences in the topsoil sample masses and, consequently, in ^{137}Cs concentration are the result of the inability to take consistent samples with 10 cm increments with the auger, especially in the top 10 cm due to the uneven, partly vegetated, soil surface. Accordingly, where activity is high, the weight of the sample had been low (a sample of highly concentrated ^{137}Cs), and vice versa (dilution of concentrated material by low concentration in lower horizons). This limitation of the auger sampling technique has no effect on the total areal activity, just how the ^{137}Cs is partitioned among horizons.

Erosion rates calculated from ^{137}Cs inventories (Table 4.5) have very large uncertainties (ca 100 %) owing to the compounding effects of the uncertainties associated with the reference value, the areal activity at the particular hillslope transect site, and the shape parameter h_0. The uncertainties are magnified further by the effects of the natural logarithm function involved in erosion calculation (compare Section 3.3.3; profile distribution model).

Table 4.5: Short-term erosion rates at transect sites derived from the profile distribution model – areal erosion rate and surface lowering rate.

	Areal Activity [Bq m^{-2}]	**Bulk Density** [g cm^{-3}]	**Areal Erosion Rate** [t ha^{-1} yr^{-1}]^{a,b}	**Lowering Rate**^{c} [m yr^{-1}]^{a,b}
S1	346	0.79	0.17	$2x10^{-4}$
S2	328	0.75	-1.24	$-2 x10^{-4}$
S3	371	0.82	1.94	$2 x10^{-4}$
S4	257	1.14	-7.42	$-7 x10^{-4}$
S5	302	1.18	-3.27	$-3 x10^{-4}$

[a] Uncertainties in the order of 100 %, [b] negative values indicate erosion, [c] Lowering rate = areal rate / bulk density

Because of the large uncertainties little emphasis can be placed on individual values, but overall there is a trend of increasing erosion rate with increasing curvature. The net deposition indicated for sites S1 and S3 is likely to be an artefact of the uncertainties arising from measurement error and spatial variability.

Assuming that each measurement is an unbiased estimate of the erosion at a site of a given curvature, a meaningful estimate of the transport coefficient K can be determined as the slope of the regression line fitted to the plot of erosion rate (lowering rate) versus curvature (Figure 4.7, compare Section 3.5).

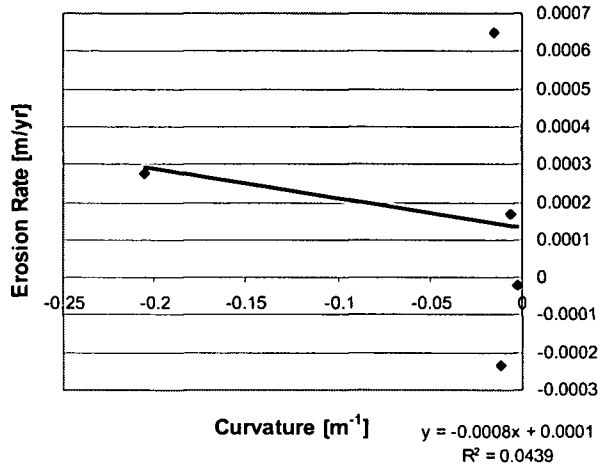

Figure 4.7: Short-term erosion rate versus total curvature for hillslope transect sites.

Table 4.6: Regression results for transport coefficient determination

	Coefficients	Standard Error	P-value
X Variable	-0.0008	0.0021	0.74

The low R^2 value (Figure 4.7) implies that curvature has little predictive power in estimating erosion rate. Additionally, the regression analysis (Table 4.6) shows not only a very high standard error but also a very low significance of the P value, meaning that it is not possible to say with any certainty that the slope is any different from zero.

4.4 Tephra profile and hillslope transect distribution

From sample point S2 to S4 the distributions of glass grains within soil profiles and along the transect (Figure 4.8) show similar patterns as in other studies where this type of tracer was used to investigate long-term transport of soil along a hillslope (e.g. Roering et al., 2002 and 2004). Each of the profiles exhibits a clear peak in glass concentration, inferred to represent the layer of tephra deposited 26,500 years BP. Downslope of S2 the depth of this peak decreases, which – as explained in Chapter 3 – indicates an increase of erosion with rising gradient and curvature (compare Section 4.1).

At S1 the depth distribution and glass concentrations are unusual (Figure 4.8a). Concentrations are typically an order of magnitude lower than at sites S2 to S4, and there is no clear explanation for these anomalies, although they might relate to strong wind sheer or

turbulence at the ridge crest that affected tephra deposition, or severe local bioturbation affecting this site. New Zealand, however, does not have deep-burrowing macro-fauna, and bioturbation by tree windthrow would not have extended to 1.8 m depth. More sites on the interfluve need to be examined to resolve this problem. The best estimate of the emplacement horizon for S1 is placed at 205 ± 10 cm, based on the fact that at the sites S2 to S4 – where a clear peak is evident – there is only a small shoulder below the peak to where the glass concentration falls to zero.

The glass concentrations at site S5 are very low and the distribution is not unimodal. The small peak in the 60-70 cm increment is not interpreted as the primary emplacement horizon.

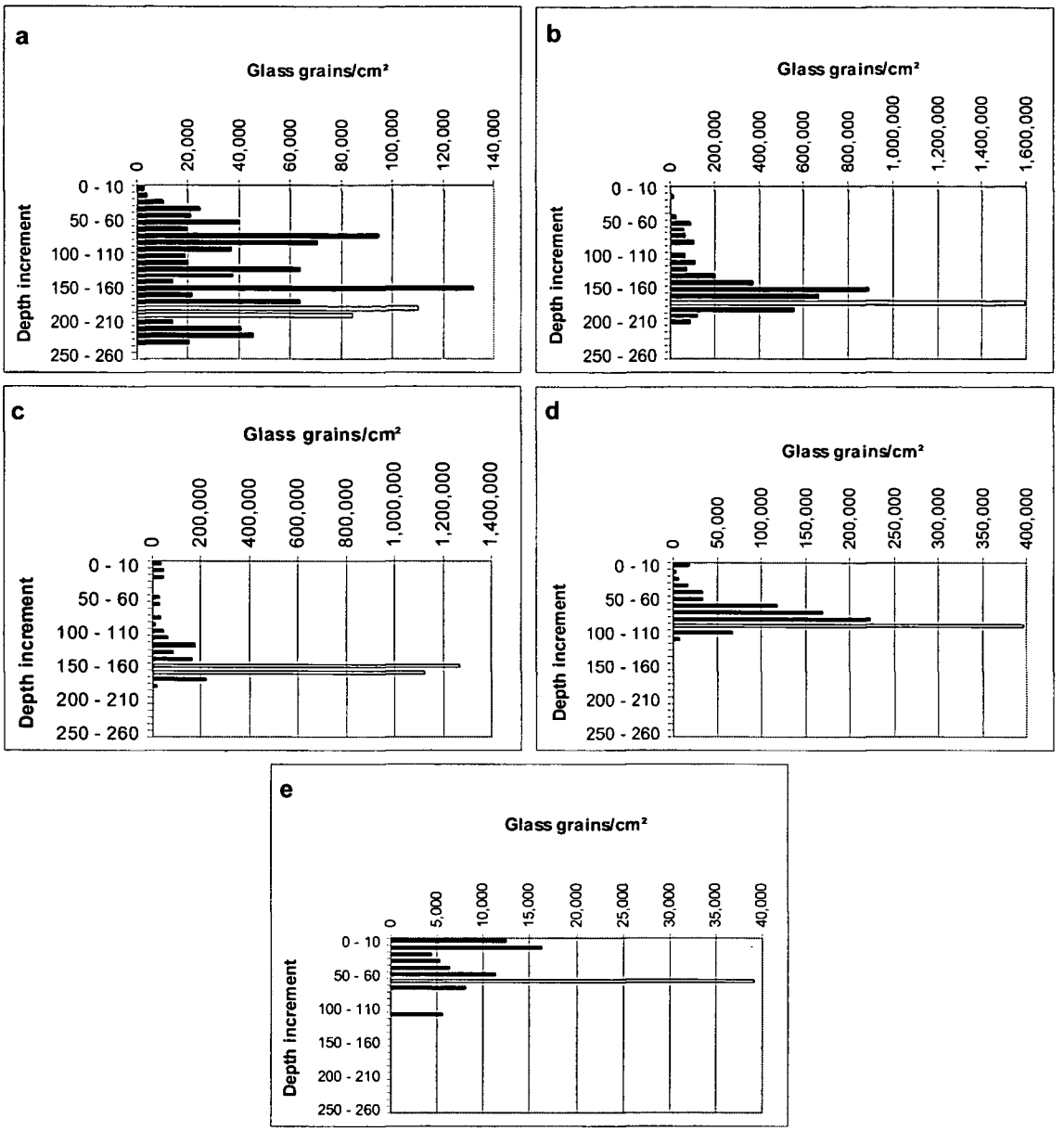

Figure 4.8: Depth profiles of glass concentration at sample sites on the hillslope transect. The tephra peak position assumed to represent the primary emplacement horizon is highlighted by hollow bars; a site 1, b site 2, c site 3, d site 4, e site 5.

4.5 Long-term erosion rates and transport coefficient K_{long}

As elaborated in Chapter 3, for the calculation of long-term erosion rates the assumption made is that the loess deposition rate, after the tephra was deposited, originally was uniform across the hillslope (Figures 2.4 and 3.1). Hence, from the difference in depth to primary emplacement horizon, between the site on the interfluve, S1, and the sloping sites, S2-S5, the total amount of erosion can be calculated using equation (1) (see Section 3.4.4) (Table 4.7).

Table 4.7: Depth [m] of tephra peak and long-term erosion rates [m yr^{-1}] at different sites

	S1	±	S2	±	S3	±	S4	±	S5	±
Peak depth	2.05	0.10	1.75	0.05	1.60	0.05	0.95	0.05	-	-
Erosion rate	0.00	0.00	$11x10^{-6}$	$2x10^{-6}$	$17x10^{-6}$	$2x10^{-6}$	$42x10^{-6}$	$2x10^{-6}$	-	-

According to the assumption that site S1, located on the interfluve, records full (uneroded) loess depth, the calculated erosion rate at this site is 0. It is not critical, however, that this assumption be correct as the calculations of the transport coefficient K_{long} below rely on differences between the amounts or the rates of erosion among sites; any error in this assumption is propagated through the analysis in such a way as to make no difference to the calculated value of K_{long}. From S2 to S4 with increasing curvature the peak depth decreases and the erosion rates augments, respectively. As explained above, at study site S5 no primary emplacement horizon could be identified, hence no erosion rate was calculated.

For the estimation of K_{long} from differences in erosion rates and curvatures from pairs of sites (equation (12) and (13)) the depth of the tephra concentration peak at different locations is compared. Table 4.8 illustrates the results of the K_{long} calculations, using estimates of hillslope convexity (curvature) and depth profiles of tephra concentration (tephra peak depth), according to equation (13). Again, S5 was not taken into consideration. The average transport coefficient is 0.0034 ± 0.0015 m^2 yr^{-1}.

Table 4.8: Long-term soil transport coefficient (K_{long}) calculation

	Δz [m]	±	ΔC [m^{-1}]	±	K [m^2 yr^{-1}]	±
S1-S2	0.30	0.15	0.0034	0.0009	0.0034	0.0027
S1-S3	0.45	0.15	0.0081	0.0017	0.0021	0.0012
S1-S4	1.10	0.15	0.0117	0.0022	0.0035	0.0012
S2-S3	0.15	0.10	0.0047	0.0019	0.0012	0.0016
S2-S4	0.80	0.10	0.0084	0.0025	0.0036	0.0017
S3-S4	0.65	0.10	0.0037	0.0033	0.0067	0.0424
				Average:	0.0034	
				SEM	0.0015	

This value was compared with the result of the graphical method of the K_{long} determination, where, as for the short-term transport coefficient, the rate of erosion was plotted against the curvature, and K_{long} was derived as the slope of the best fitting line (Figure 4.9, compare Section 3.5). It can be seen that both methods achieve similar results (0.0034 ± 0.0015 m^2 yr^{-1} vs. 0.0032 ± 0.0007 m^2 yr^{-1}).

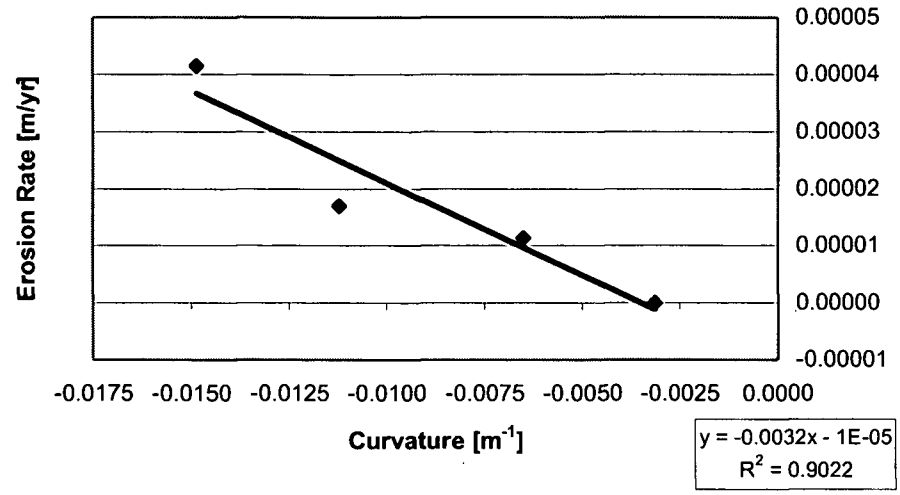

Figure 4.9: Long-term erosion rate versus total curvature for hillslope transect sites.

It can be noticed that the intercept is negative in this graph, e.g. negative erosion (accumulation) when the curvature is zero. This originates from the assumption that no erosion has happened at S1, despite the fact that this site has non-zero convexity. This offset does not affect the value of K_{long}. The results from the multiple regression (K_{long} = 0.0032 ± 0.0007 m^2 yr^{-1}; Figure 4.9 and Appendix 7) illustrates that although both methods are appropriate to determine the transport coefficient K_{long} the latter achieves higher accuracy due to a lower uncertainty in the estimate (SEM 0.0015 vs. 0.0007).

5 DISCUSSION

5.1 Slope morphology

The hillslope studied shows a progressive increase in profile curvature from the hilltop to site S4, 66 m downslope (Table 4.1). From site S4 to site S5 profile curvature increased markedly, although a much smaller radius of influence (2.5 m) was used to calculate curvature at the lower site. This was done because the local microtopography of gullies and spurs was assumed to be driving erosion. Using a larger search radius (7.5-15 m), profile curvature for site S5 is very similar to site S4. Gradient at site S5 is 0.35, close to the threshold value of 0.4 identified by Roering et al. (2002) as the gradient beyond which soil transport increases non-linearly with increasing gradient, and hence soil erosion becomes insensitive to increasing curvature. Ignoring the local plan curvature created by the evolving tunnel gullies near site S5 the hillslope studied appears to be one of uniformly increasing curvature (Table 4.1, Appendix 1) (Mudd and Furbish, 2006). This indicates a non-equilibrium condition because increasing curvature downslope drives increasing erosion rate. In other words, the lower sideslopes of the hillslope are eroding faster than the hill crest. A pattern of increasing downslope curvature is an indication usually of a transient erosional response driven by accelerated base-level lowering at the toe of the slope. Presently, the valley floor the studied hillslope grades to is filled by Holocene alluvium and therefore base level lowering is not presently active. This suggests the increasing convexity in a downslope direction is, to a large extent, inherited from the slopes formed across the underlying basalt beneath the loess mantle. The valley slopes in the study area appear to be in a non-steady condition, reflecting lags in hillslope response to base level controls including valley downcutting in glacial times, and valley aggradation in the postglacial (Shulmeister et al., 1999), and modification of the regolith on the slopes by loess accumulation in the last glaciation (Almond et al., 2007). The progressive increase in profile curvature (when measured at larger spatial scales) also suggests that the present gully and spur microtopography at site S5 is a relatively recent modification of the slope engendered by upslope propagation of tunnel gullies.

5.2 Comparison of long-term and short-term erosion rates

Long-term erosion rates, as quantified by tephra distribution along the hillslope, appear to be proportional to hillslope curvature, confirming the appropriateness of a slope dependent transport model. The transport coefficient calculated over the long term (K_{long} = 0.0032 ± 0.0007 m^2 yr^{-1}) is lower by a factor of about 4 than that estimated for the Charwell area in north Canterbury, New Zealand, over the identical period from deposition of Kawakawa

tephra to present (Roering et al., 2002). Walther (2006) determined a transport coefficient of 0.007 ± 0.002 m^2 yr^{-1} on a hillslope in eastern Washington over the time period from deposition of Mazama ash (7.600 cal yr BP) to the present. Over this time vegetation was dominantly coniferous forest. Using the Charwell data set, Roering et al. (2004) modelled the distribution and concentration of glass grains in the soil profiles of the Charwell area and concluded the value of the transport coefficient varied from ca 0.002 m^2 yr^{-1} under glacial grasslands to 0.016 ± 0.005 m^2 yr^{-1} under Holocene forest. They attributed this increase to a more rigorous bioturbation regime under forest than grassland that promotes more vigorous soil transport.

An examination of the redistribution of glass grains adjacent to the tephra peak in the present study provides some indication of erosion under glacial conditions at Ahuriri. The significant dilution of glass grains that occurs in a downslope direction (neglecting site S1 for reasons discussed above) (Table 5.1) is evidence of erosion diluting glass concentration by incorporating tephra-free loess from the underlying substrate. This erosion must have occurred from the time of deposition of Kawakawa tephra to when loess accumulation was thick enough to effectively isolate the tephra from further erosion.

Table 5.1: Peak inventory (± 30 cm of highest grain count) and total glass inventory at sample sites S1-S5

	S1	S2	S3	S4	S5
Peak glass	377,870	4,291,789	3,053,575	983,066	70,087
Total glass	8,875,503	44,964,795	29,895,817	9,642,491	956,885

The lower average value of K_{long} at Ahuriri than at Charwell suggests a different vegetation history between the two sites. The lower rainfall at Ahuriri (690 mm MAR versus ca 1400 mm MAR at Charwell) may have delayed the postglacial reforestation at Ahuriri relative to Charwell and perhaps limited the stature of the forest that grew.

Any difference between long-term erosion rate and short-term erosion rate would be captured in differences in K_{long} and K_{short}. Unfortunately, the level of variability of the ^{137}Cs-based short-term erosion rates does not allow an assessment of the appropriateness of the slope-dependent transport model over the short term, and it prevents a meaningful estimate of K_{short} being made. Assuming little difference between ^{137}Cs areal activities at sites IF1-4, IF5-8, S1, S2, and S3 due to erosion, the standard deviation and CV are 31 Bq m^{-2} and 9 %, respectively. These values are consistent with variability reported in the literature (e.g. Basher, 2000), which is largely attributed to spatial variability of original ^{137}Cs deposition. An analysis of

power of the regression analysis (Table 4.6) suggests as many as 20 observations would be necessary to determine a statistically significant slope (at 95 % confidence) when K_{short} is approximately equal to K_{long}. If K_{short} was higher, fewer observations would be necessary.

An alternative approach to comparing short- and long-term erosion rates is to use K_{long} (0.0032 ± 0.0007 m^2 yr^{-1}) in equation (4) with the known curvatures to estimate erosion rates at the hillslope transect sites to allow a visual comparison with the ^{137}Cs-based short-term erosion rate estimates (Figure 5.1).

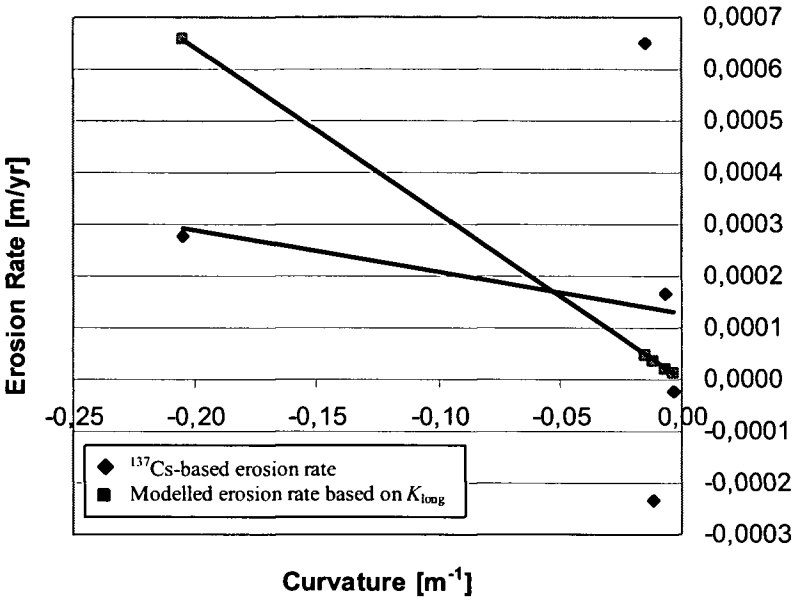

Figure 5.1: Erosion rate estimated from the long-term transport coefficient (K_{long}) and from ^{137}Cs inventory versus curvature.

The large amount of noise in the ^{137}Cs-derived erosion rates again makes it difficult to draw unequivocal conclusions. Focussing on the erosion rate at S5, however, where curvature is highest at ca -0.2 m^{-1}, it appears that the present erosion rate here is not higher than the expected long-term average rate.

In comparison with other ^{137}Cs-based measurements of recent soil loss in New Zealand, the maximum erosion rate at this site (0.0007 m yr^{-1} = 7.4 t ha^{-1} yr^{-1} at S4, Table 4.5) is still generally lower than under more intensive land uses on far less steeply sloping land. Basher et al. (1995, 1997, 2002, and 2004) estimated mean soil loss as 11-17 t ha^{-1} yr^{-1} on cropped fields (Canterbury, Manuwatu), 5-30 t ha^{-1} yr^{-1} under intensive commercial vegetable production (Pukekohe, Ohakune), and as 19-51 t ha^{-1} yr^{-1} as an effect of mouldboard ploughing (South Canterbury; Quine et al., 2003). The maximum value estimated in these studies was 145 t ha^{-1}

yr^{-1} on a field under intensive carrot production in Ohakune in central North Island. Clearly, the grass sward at the study site, despite thinning and dying during summer droughts, is still resilient enough to prevent large soil losses from rainsplash and other creep processes.

In the Northern Hemisphere similar estimates were determined. Theocharopoulos et al. (2003) calculated values of ~ 22 t ha^{-1} yr^{-1} for a cultivated catchment area in Greece, Yang et al. (2006) estimated soil loss as > 25 t ha^{-1} yr^{-1} on cultivated interfluve slopes in the Loess Plateau of China, and Li et al. (2007) received estimates of ~ 22 t ha^{-1} yr^{-1} on agricultural hilly areas in the North American Great Plains. On uncultivated land, Porto et al. (2003) calculated estimates of 22-30 t ha^{-1} yr^{-1} in two forested catchments in Calabria, Italy.

Similarly to the ^{137}Cs analysis, where the total inventory of areal activity at the reference sites is not significantly higher than at the sites along the slope, also the properties of tephra distribution show anomalies. As elaborated in chapter 4.3, contrary to the assumption that the total amount of tephra at site S1 would be slightly higher than, or in the range of, study site S2 (~ 45 x 10^{-6}), at the site located on the interfluve only ~ 9 x 10^{-6} glass grains were found. Also the pattern that the tephra peak is composed of ca 10 % of the total glass inventory does not apply to site S1 where it is less than 5 %. The coincidence of anomalies in the ^{137}Cs and the tephra analysis leads to the suggestion that the location on the interfluve, and consequently a particular exposure to impact of wind or rain splash, had a considerable influence on the deposition of tephra 26,500 years ago as well as of ^{137}Cs from the 1950s to the 1990s when the radionuclide precipitation ceased (compare Section 4.4). Especially in the case of ^{137}Cs this coherence seems plausible, because of the fact that this radionuclide got to the earth surface by rainfall.

5.3 Sources of uncertainty and limitations

For the determination of short- and long-term erosion rates the approaches used have been already applied in various studies and their functioning proven. Nonetheless, in order to see the results in the right context, it is necessary to bear in mind the limitations of the approach and uncertainties inherent in a few procedural steps of the present study.

5.3.1 ^{137}Cs technique

Concerning the auger technique for sampling, it has to be stated that problems like material falling into the hole while withdrawing the auger, reduced control over sampling depth, root and stone obstacles, and material dislodged from the walls of the hole may arise (Zapata,

2000). These problems, as well as the possibility of varying sample volumes, were avoided as much as possible by especially careful sampling.

As mentioned earlier, Basher (2000) underlines the importance of an adequate characterisation of natural variability, advocating a minimum of 10-15 samples per site to relatively precisely estimate the mean areal activity at the reference site. While an intense sampling would adequately quantify the magnitude of variability, it would tell us nothing about the spatial structure of the variation due to the initial pattern of ^{137}Cs deposition. The approach of quantifying the ^{137}Cs inventory at each site in this study by using four cores probably quantifies adequately the local site ^{137}Cs inventory. However, unless spatial variability has very short range (< 1 m), even if the rate of erosion was the same at two sites of identical curvature, spatial variability in original ^{137}Cs deposition would result in a different estimate of erosion rate. This kind of variability appears to be the source of the very low R^2 value in the regression of curvature versus erosion rate (Table 4.6, Figure 4.7). This variability also confounds determination of a statistically significant slope, or, related to this, a low standard error of the slope. In order to identify a statistically significant difference between K_{long} and K_{short}, either more observations would need to be taken to increase the statistical power of the regression, or alternatively enough discrimination could be provided with the present number of observations if K_{short} was much greater than K_{long}, e.g. the short-term erosion rate versus curvature curve was much steeper than that of the long term plot.

Another point that deserves attention is that the ^{137}Cs technique does not allow for the documentation of short-term changes in erosion rates such as those related to changes in land use and management practices since the first deposition of ^{137}Cs (compare Chapter 1). That was why in the present study an area was chosen for which it can be assumed with a high level of certainty that no such changes have occurred during the last decades. The depth profile of ^{137}Cs distribution at the reference site IF1-4 and the similarity of the shape parameter, h_0, to those reported in the literature support the assumption of a relatively undisturbed ^{137}Cs profile, and the adoption of the profile distribution conversion model for calculating erosion rates.

5.3.2 Tephra analysis

During subsampling and sample preparation the aim was to achieve unbiased but representative samples for each sample interval. Nonetheless, a risk of reduction or potential loss of accuracy due to these treatments and the averaging of the data over relatively coarse

sampling increments (10 cm) remains. In the case of the tephra marker bed approach, Walther (2006) points out the risk of a slight change in the location of the tephra peak due to the use of discrete sample increments, leading to uncertainties in the differences between the peak depths. Connected to that is the potential source of error lying in the assumption that the artificial beads used in the spiking technique are homogenously mixed into the samples.

An issue in the context of the determination of the transport coefficient K_{long} in the tephra analysis is the fact that the deposition of loess on top of the tephra is assumed to have occurred in a quite short time frame, leading to a clearly recognisable primary depositional layer of tephra, which then establishes a depth and time datum. As discussed before, this assumption seems to be problematic at least on the interfluve of the hillslope, where it seems that redistribution processes occurred already during the period of tephra deposition.

In addition to these influences on the depth of tephra peaks and, consequently, on the differential erosion values, another source of uncertainty lies in the determination of the topographic properties of the hillslope and, in context of the K values, of the curvature respectively. On the one hand the overall topography has undoubtedly experienced some changes during the time frame observed. On the other hand the interpolation of the hillslope surface using a second-order polynomial holds the danger of smoothing actual irregularities that are important to ^{137}Cs redistribution. This issue was met by the use of various point sets (within five different radii) for the calculation of gradient and curvature, in order to test the variability of these topographic parameters and to reduce the dimension of influencing local noise. One of the greatest concerns is the somewhat arbitrary adoption of the shortest range of influence (2.5 m) for determining the curvature for the lowest site, S5. The validity of this decision depends largely on the length of time the gullies and spurs formed by propagating tunnel gullies have existed relative to the time frame of ^{137}Cs deposition. Analysis of old aerial photographs would provide a better basis for the selection of search radius.

5.4 Implications

The purpose of the present study is the quantification and the comparison of the natural rates of erosion at different time scales, in order to be able to assess the severity of anthropogenically induced soil erosion. In addition to the above mentioned possibility of getting more significant results for short-term erosion rates using more measurement points for the ^{137}Cs analysis, other techniques could deliver an interesting supplement to the present study. Direct methods like erosion pins do not seem to be adequate, as the lowering rate

appears to be too low as to show short-term results. Similarly, a regular survey of the slope surface using high resolution GPS might not be sensitive enough as to determine a lowering rate of < 5 cm in 50 years.

Yet, other radionuclides could be used to quantify short-term erosion rates. Zapata (2003) mentions various gamma ray emitters (^{59}Fe, ^{46}Sc, ^{110}Ag, ^{198}Au, ^{137}Cs, ^{51}Cr) which can be used to determine extend and source of soil loss by so-called artificial labelling of soil particles. He also specifies various environmental radionuclides in addition to fallout ^{137}Cs, such as natural ^{210}Pb and cosmogenic ^{7}Be (compare Section 1.2.2.1), and others ($^{239-240}$Pu, ^{14}C, ^{32}Si, ^{26}Al, ^{36}Cl, etc.) which, according to the needed time scale, can be used for the assessment of soil erosion. VandenBygaart (2001) examined the deposition history of an agricultural field in southern Ontario, Canada, deriving it from the depth-stratigraphy of ^{137}Cs and soil organic carbon (SOC). Wallbrink et al. (2002) combined measurements of particle-bound radionuclides (^{137}Cs, ^{210}Pb, ^{226}Ra, ^{232}Th and ^{40}K) and classical geomorphology for the investigation and reconstruction of the different phases of development of a gully in the Stavropol region in southern Russia during the last ~ 50 years. Despite the inapplicability in the present study because of the lack of trees in the study area, the approach of Mizugaki et al. (2006) seems promising for sedimentation studies. To examine the effects from changes in land use and river canalisation, reflected in recent changes in sedimentation rates in Kushiro Mire, Northern Japan, dendrogeomorphology (analysis of tree growth responding to geomorphic processes) and ^{137}Cs and ^{210}Pb were used.

Actually, rather than on the upper part of convex hillslopes, significant erosion processes seem to be concentrated in areas of tunnel gullies on the lower backslopes and incised valleys on the ridges of Banks Peninsula. These tunnel gullies are propagating back up and lead to evident soil loss. To quantify the dimension of this soil loss, further studies either on the same ridge or on similar ridges could be carried out using e.g. the above mentioned techniques or volumetric analysis of the sediment fan at the outlet of a gully. This would also enable to get more insights in the sediment yield of such a ridge and probably in the quantitative relation between soil loss on the upper backslope an in the gullies, as shown by Li et al. (2003) who used the ratio between unsupported ^{210}Pb and ^{137}Cs for this purpose.

With respect to the applied tephra tracer technique an interesting aspect would be to determine the exact transition dates from forest to grass vegetation, and vice versa, in the present study area, as elaborated by Shulmeister et al. (1999), Roering et al. (2002, 2004),

etc., in order to find out when erosivity patterns might have changed. With this information also changes in topography could be simulated, similar to the study carried out by Roering et al. (2004) who used a coupled model for the transport of soil and tracer particles at the hillslope scale, and two equally recent studies by Collins et al. (2004) and Istanbulluoglu and Bras (2005) who examined the effects of vegetation on landscape processes, drainage density, and on topography using the CHILD model. This model imitates landscape evolution by simulation of discrete rainfall events, taking into account various geomorphic processes, such as fluvial erosion, hillslope diffusion, or tectonic uplift. The theory behind this approach is that the "composition" of climate, soil type and topography evokes a certain type of vegetation, whereas vegetation, for its part, influences hydraulic and geomorphic processes in basins, or on the level of whole landscapes. In this way gathered topographic data could then be used to prove the assumption that the present hillslope morphology is similar to the one 26,500 years ago. Additionally, the parameters for the transport model used in the present study could be refined, in order to receive more differentiated results.

Finally, studies similar to the present one but carried out in neighbouring incisions (valleys or gullies), and with similar or different cultivation or grazing history, could help in proving if and where human activity has had an impact on erosion processes on Banks Peninsula.

6 CONCLUSION

The quantification and comparison of long-term and short-term erosion rates is the only way to assess the effect of anthropogenic land use changes on the severity of soil erosion and hence the sustainability of the present land use – in the present study on Banks Peninsula, in the South Island of New Zealand.

A convex soil-mantled hillslope was chosen, where forest that persisted before the arrival of Europeans was replaced with introduced grassland. In the present subhumid climate this grassland is susceptible to drought especially in summer, and its deterioration at this time opens up the soil to influences of rainsplash that may not have occurred under the original forest cover.

Convex hillslopes form under conditions of slope-dependent soil transport which can be modelled as $\widetilde{q}_s = -K^* \partial z / \partial x$, where K is the transport coefficient which quantifies the power of soil disturbance and transport mechanisms. With soil transport obeying this law, erosion is dependent on slope curvature $E = K^* \partial^2 z / \partial x^2$.

Short-term soil erosion was assessed using bomb-fallout ^{137}Cs, whose redistribution across the landscape can be used to determine soil erosion and deposition. Long-term soil erosion was measured using the depth to primary emplacement horizon of a 26,500 year tephra. Five sites along a linear hillslope transect with increasing curvature were selected and sampled for ^{137}Cs and tephra analysis. Erosion rates at the sites of different curvature were used to calibrate transport models relevant to the two time scales. Differences in short-term and long-term erosion should be manifested as differences in K at two timescales (K_{short}, K_{long}).

The estimate for K_{long} resulted in 0.0032 ± 0.0007 m^2 yr^{-1}. This result of the tephra analysis is lower by a factor of about 4 than that estimated for the Charwell area in north Canterbury, New Zealand, over the identical period from deposition of Kawakawa tephra to present (Roering et al., 2002), and half as high as the transport coefficient of a similar study carried out on a hillslope in eastern Washington over the time period from deposition of Mazama ash (7.600 cal yr BP) to the present (Walther, 2006), probably due to different vegetation cover histories.

Due to the variability in the ^{137}Cs data and to the little extent of erosion in the short time scale, K_{short}, the short-term transport coefficient, could not be determined. Nevertheless, there was no evidence to suggest that it is any greater than K_{long}, which would have indicated an increase in soil erosion efficiency from the long to the short time scale. In comparison to other recent erosion rates measured by ^{137}Cs on arable lands the present erosion rate is generally well lower. High erosion rate occurs lowest on the upper backslope, where the closely spaced gullies have accentuated local curvature and erosion. Below this point these tunnel gullies are actively transporting sediment and this is probably the major locus of erosion in the landscape. Hence, based on the findings of the present study and on the experiences made with the applied techniques, future research should be aiming for the refining of the used techniques and for the quantification of tunnel-gully erosion.

7 REFERENCES

Abrahams, A. D., Parsons, A. J., Hirsch, P. J. (1992). Field and laboratory studies of resistance to interrill overland flow on semi-arid hillslopes, southern Arizona. In Parsons, A. J. and Abrahams, A. D. (Ed). *Overland Flow. Hydraulics and erosion mechanics* (pp. 1-24). London, U.K.: UCL Press.

Almond, P. C., Shanhun, F. L., Rieser, U., Shulmeister, J. (2007). An OSL, radiocarbon and tephra isochron-based chronology for Birdlings Flat loess at Ahuriri Quarry, Banks Peninsula, Canterbury, New Zealand. *Quaternary Geochronology 2*(1-4), 4-8.

Bacchi, O. O. S., Reichardt, K., Sparovek, G. (2003). Sediment spatial distribution evaluated by three methods and its relation to some soil properties. *Soil & Tillage Research 69*, 117-125.

Basher, L. R., Matthews, K. M., Zhi, L. (1995). Surface erosion assessment in the South Canterbury downlands, New Zealand using ^{137}Cs distribution. *Australian Journal of Soil Resources 33*, 787-803.

Basher, L. R. and Webb, T. H. (1997). Wind erosion rates on terraces in the Mackenzie Basin. *Journal of the Royal Society of New Zealand 27*(4), 499-512.

Basher, L. R. (2000). Surface erosion assessment using ^{137}Cs: examples from New Zealand. *Acta Geologica Hispanica 35*(3-4), 219-228.

Basher, L. R. and Ross, C. W. (2002). Soil erosion rates under intensive vegetable production on clay loam, strongly structured soils at Pukekohe, New Zealand. *Australian Journal of Soil Resources 40*, 947-961.

Basher, L. R., Ross, C. W., Dando, J. (2004). Effects of carrot growing on volcanic ash soils in the Ohakune area, New Zealand. *Australian Journal of Soil Resources 42*, 259-272.

Bryan, R. B. (2002). Soil erodibility and processes of water erosion on hillslope. *Geomorphology 32,* 385-415.

Collins, D. B. G., Bras, R. L., Tucker, G. E. (2004). Modelling the effects of vegetation-erosion coupling on landscape evolution. *Journal of Geophysical Research 109*, F03004.

Cuff, J. R. I. (2006). *Progress report on monitoring soil erosion on arable land using the ^{137}Caesium method in 2005/2006.* Environment Canterbury technical report. Environment Canterbury, Christchurch, New Zealand.

Dietrich, W. E., Reiss, R., Hsu, M.-E., Montgomery, D. R. (1995). A process-based model for colluvial soil depth and shallow landsliding using digital elevation data. *Hydrological Processes 9*, 383-400.

Dietrich, W. E., Bellugi, D. G., Heimsath, A. M., Roering, J. J., Sklar, L. S., Stock, J. D. (2003). Geomorphic transport laws for predicting landscape form and dynamics. Prediction in Geomorphology. *Geophysical Monograph 135*, © 2003 by the American Geophysical Union.

Ducey, C. (2001). *A quantitative method to assess volcanic glass content in soils.* Honors Project, University of Oregon, U.S.A..

Eyles, G. O. (1983). The distribution and severity of present soil erosion in NZ. *NZ Geographer 39*(1), 12-28.

Florineth, F. and Rauch, H. P. (2001). *Ingenieurbiologie.* Unpublished study records.

Gilbert, G. K. (1909). The convexity of hilltops. *Journal of Geology 17*, 344-350.

Graf, C., Böll, A., Graf, F. (2003). *Pflanzen im Einsatz gegen Erosion und oberflächennahe Rutschungen.* Merkblatt fuer die Praxis 37 - Eidgenössische Forschungsanstalt WSL.

Gray, D. A. and Sotir, R. B. (1996). *Biotechnical and soil bioengineering slope stabilization - A practical guide for erosion control.* N.Y., U.S.A.: John Wiley & Sons Inc..

Griffiths, E. (1973). Loess on Banks Peninsula. *N.Z. Journal of Geology and Geophysics 16*, 657-675.

Griffiths, E. (1974). *Soils of parts of the port hillsand adjacent plains, Canterbury, New Zealand.* Soil Bureau Bulletin 35. New Zealand Department of Scientific and Industrial Research. Wellington, New Zealand: A. R. Shearer, Government Printer.

Heimsath, A. M., Chappell, J., Spooner, N. A., Questiaux, D. 1. G. (2002). Creeping soil. *Geology 30*(2), 111-114.

Istanbulluoglu, E. and Bras, R. L. (2005). Vegetation-modulated landscape evolution: Effects of vegetation on landscape processes, drainage density, and topography. *Journal of Geophysical Research 110*, F02012.

Kangas, P. C. (2004). *Ecological engineering - Principles and practice.* Boca Raton, U.S.A: CRC Press LLC.

Köppen, W. (1931). *Grundriss der Klimakunde.* Berlin, GER: Walter de Gruyter & Co.

Lal, R., Blum, W. H., Valentine, C., Stewart, B. A. (1998). *Methods for assessment of soil degradation.* Boca Raton, U.S.A.: CRC Press LLC.

Li, Y., Poesen, J., Yang, J.C., Fu, B., Zhang, J.H. (2003). Evaluating gully erosion using ^{137}Cs and $^{210}Pb/^{137}Cs$ ratio in a reservoir catchment. *Soil & Tillage Research 69*, 107-115.

Li, S., Lobb, D. A., Lindstrom, M. J., Farenhorst, A. (2007). Tillage and water erosion on different landscapes in the northern North American Great Plains evaluated using ^{137}Cs technique and soil erosion models. *Catena* (in press). 01167, 13 pages.

Matthews, K. M. (1989). *Radioactive fallout in the South Pacific: a history.* Part 1: Deposition in New Zealand. Report NRL 1989/2, National Radiation Laboratory, Christchurch, New Zealand.

Mizugaki, S., Nakamura, F., Araya, T. (2006). Using dendrogeomorphology and ^{137}Cs and ^{210}Pb radiochronology to estimate recent changes in sedimentation rates in Kushiro Mire, Northern Japan, resulting from land use change and river channelization. *Catena 68*, 25-40.

Morgan, R. P. C. (2005). *Soil Erosion and Conservation.* Malden, U.S.A.; Oxford, U.K., Carlton, Australia: Blackwell Publishing.

Mudd, S. M. and Furbish, D. J. (2006). Using chemical tracers in hillslope soils to estimate the importance of chemical denudation under conditions of downslope transport. *Journal of Geophysical Research-Earth Surface 111.* F02021, DOI:10.1029/2005JF000343.

Pan, C., Shangguan, Z., Lei, T. (2006). Influences of grass and moss on runoff and sediment yield on sloped loess surfaces under simulated rainfall. *Hydrological Processes* (in press). Published online on Wiley InterScience (www.interscience.wiley.com). DOI: 10.1002/hyp.6158

Parker, G. G. (1963): Piping, a geomorphic agent in landform development of the drylands. *International Association of Hydrological Sciences Publications 65*, 103-113.

Parsons, A. J. and Abrahams, A. D. (1992). *Overland Flow. Hydraulics and erosion mechanics.* London, U.K.: UCL Press.

Pennock, D. J. and Appleby, P. G. (2002). Sample Processing. In Zapata, F. (Ed.). *Handbook for the assessment of soil erosion and sedimentation using environmental radionuclides* (pp. 59-65). Dordrecht, NL: Kluwer Academic Publishers.

Poesen, J. Vandekerckhove, L., Nachtergaele, J., Oostwoud Wijdenes, D., Vestraeten, G., van Wesemael, B. (2002). Gully erosion in dryland environments. In Bull, L. J., Kirkby, M. J. (Eds.), *Dryland Rivers: Hydrology and Geomorphology of Semi-Arid Channels* (pp. 229-262), Chichester: U.K.: John Wiley and sons.

Poesen, J., Nachtergaele, J., Verstraeten, G., Valentin, C. (2003). Gully erosion and environmental change: importance and research needs. *Catena 50*, 91-133.

Porto, P., Walling, D. E., Ferro, V. Di Stefano, C. (2003). Validating erosion rate estimates provided by caesium-137 measurements for two small forested catchments in Calabria, southern Italy. *Land Degradation & Development 14*, 389-408.

Quine, T. A., Basher, L. R., Nicholas, A. P. (2003). Tillage erosion in the South Canterbury Downlands, New Zealand. *Australian Journal of Soil Resources 41*, 789-807.

Reijman, J., Turski, R., Paluszek, J. (1998). Spatial and temporal variations in erodibility of loess soil. *Soil & Tillage Research 46*, 61-68.

Reneau, S. L. and Dietrich, W. E. (1991). Erosion rates in the southern Oregon Coast Range: Evidence for an equilibrium between hillslope erosion and sediment yield. *Earth Surface Processes and Landforms 16*, 307-322.

Ritchie, J. C. and McHenry, J. R. (1990). Application of radioactive fallout cesium-137 for measuring soil erosion and sediment accumulation rates and patterns: a review. *Journal of Environmental Quality 19*, 215-233.

Robertson, N. G. (1956). The delineation of natural areas in New Zealand: Climatic districts in New Zealand. Report to annual meeting of New Zealand Ecological Society. *Proceedings of the New Zealand Ecological Society 4.*

Roering, J. J., Kirchner, J. W., Dietrich, W. E. (1999). Evidence for nonlinear, diffusive sediment transport on hillslopes and implications for landscape morphology. *Water Resource Research 35*(3), 853-870.

Roering, J. J., Almond, P., Tonkin, P., McKean, J. (2002). Soil transport driven by biological processes over millennial time scales. *Geology 30*(12), 1115-1118.

Roering, J. J., Almond, P., Tonkin, P., McKean, J. (2004). Constraining climatic controls on hillslope dynamics using a coupled model for the transport of soil and tracers: Application to loess-mantled hillslopes, South Island, New Zealand. *Journal of Geophysical Research 109*, F01010.

Roering (2004). Soil creep and convex-upward velocity profiles: theoretical and experimental investigation of disturbance-driven sediment transport on hillslopes. *Earth Surface Processes and Landforms 29*, 1597-1612.

Schiechtl, H. and Stern, R. (2002). *Naturnaher Wasserbau. Anleitung für ingenieurbiologische Bauweisen*. Berlin, GER: Ernst.

Selby, M. J. and Hodder, A. P. W. (1993). *Hillslope materials and processes*. Oxford, England: Oxford University Press.

Sewell, R. J., Weaver, S. D., Reay M. B. (1993). *Geology of Banks Peninsula*. Lower Hutt, N.Z.: Institute of Geological and Nuclear Sciences.

Shanhun, F. (2004). *Soil stratigraphy and chemistry of the Birdlings Flat Formation loess and Ahuriri Quarry, Canterbury*. Honours dissertation, Lincoln University, Christchurch, New Zealand.

Shulmeister, J., Soons, J. M., Berger, G. W., Harper, M., Holt, S., Moar, N., Carter, J. A. (1999). Environmental and sea-level changes on Banks Peninsula (Canterbury, New

Zealand) through three glaciation-interglaciation cycles. *Palaeogeography, Palaeoclimatology, Palaeoecology 152*, 101-127.

Soil Science Society of America (2001). *Glossary of soil science terms*. Retrieved September 26, 2006, from http://www.soils.org/sssagloss/index.php

Song W., Liu P. L., Yang M. Y., Xue Y. Z. (2003). Using REE tracers to measure sheet erosion changing to rill erosion. *Journal of Rare Earths 21*(5), 587-590.

Theocharopoulos, S. P., Florou, H., Walling, D. E., Kalantzakos, H., Christou, M., Tountas, P., Nikolaou, T. (2003). Soil erosion and deposition rates in a cultivated catchment area in central Greece, estimated using the 137Cs technique. *Soil & Tillage Research 69*, 153-162.

Trangmar, B. B. and Cutler, E. J. B. (1983): *Soils and erosion of the Sumner region of the Port Hills, Canterbury, New Zealand.* New Zealand Soil Survey Report 70, 52.

Tschang, H. L. (1972). Geomorphical observations on rainwash forms in Hong Kong and some other humid regions of Southeast Asia. *Chung Chi Journal 11*(1), 40-59.

Tufts University (2006). *Banks Peninsula*. Photo retrieved September 26, 2006, from http://www.tufts.edu/~crogers/NZ/Akaroa.png

VandenBygaart, A. J. (2001). Erosion and deposition history derived by depth-stratigraphy of ^{137}Cs and soil organic carbon. *Soil & Tillage Research 61,* 187-192.

Wainwright, J., Parsons, A. J., Abrahams, A. D. (2000). Plot-scale studies of vegetation, overland flow and erosion interactions: case studies from Arizona and New Mexico. *Hydrological Processes 14*, 2921-2943.

Wallbrink, P. J., Belyaev, V., Golosov, V., Sidorchuk, A. S., Murray, A. S. (2002). *Use of radionuclide, field based and erosion modeling methods for quantifying rates and amounts of soil erosion processes*. 2002, CSIRO Land and Water Consultancy Report.

Wallbrink, P.J. Walling, D.E. and He. Q. (2002). Radionuclide measurement using HpGe gamma spectrometry. In Zapata, F. (Ed.). *Handbook for the assessment of soil erosion and sedimentation using environmental radionuclides* (pp. 67-97). Dordrecht, NL: Kluwer Academic Publishers.

Walling, D.E. and Quine, T.A. (1993). *Use of caesium-137 as a tracer of erosion and sedimentation: handbook for the application of the caesium-137 technique.* UK Overseas Development Administration Research Scheme R4579. Exeter, U.K.: Department of Geography, University of Exeter.

Walther, S. C. (2006). *Quantifying biogenic sediment transport on a forested, loess- mantled hillslope in the Blue Mountains, eastern Washington.* Masters Thesis, University of Oregon, U.S.A..

Wilson, C. J. N., Switsur, V. R., Ward, A. P. (1988). A new C-14 age for the Oruanui (Wairakei) eruption, New Zealand. *Geological Magazine 125*(3), 297-300.

Wilson, C. J. N. (2001). The 26.5 ka Oruanui eruption, New Zealand: an introduction and overview. *Journal of volcanology and geothermal research 112*(1-4), 133-174.

Wilson, H. D. (1992). *Banks ecological region. Port Hills, Herbert and Akaroa ecological districts.* Protected natural areas programme - survey report no. 21. Christchurch, N.Z.: Canterbury Conservancy, Department of Conservation, private bag.

Wilson, H. D. (1998). Living in Raoul country: the changing flora and vegetation of Banks Peninsula. In Burrows, C. J. (1998) *Etienne Raoul and Canterbury Botany 1840-1996.* Christchurch, N.Z.: Canterbury Botanical Society & Manuka Press.

Xinxiao, Y., Xuexia, Z., Jianlao, L. Manliang, Z. Yuanyuan, X. (2006). Effects of vegetation cover and precipitation on the process of sediment produced by erosion in a small watershed of loess region. *Acta Ecologica Sinica 26*(1), 1−8.

Yang, M. Y., Walling, D. E., Tian, J. L., Liu, P. L. (2006). Partitioning the contributions of sheet and rill erosion using Beryllium-7 and Cesium-137. *Soil Science Society of America Journal 70*, 1579-1590.

Zapata, F. (2002). *Handbook for the assessment of soil erosion and sedimentation using Environmental Radionuclides.* Dordrecht, NL: Kluwer Academic Publishers.

Zapata, F., Garcia-Agudo, E., Ritchie, J. C. and Appleby, P. G. (2002). Introduction. In Zapata, F. (2002). *Handbook for the Assessment of Soil Erosion and Sedimentation Using Environmental Radionuclides.* Dordrecht, NL: Kluwer Academic Publishers.

Zapata, F. (2003). The use of environmental radionuclides as tracers in soil erosion and sedimentation investigations: recent advances and future developments. *Soil & Tillage Research 69*, 3-13.

Zhu, T. X. (1997). Deep-seated, complex tunnel systems a hydrological study in a semi-arid catchment, Loess Plateau, China. *Geomorphology 20,* 255-267.

Zhu, T. X., Cai, Q. G., Zeng, B. Q. (1997). Runoff generation on a semi-arid agricultural catchment: field and experimental studies. *Journal of Hydrology 196,* 99-118.

Zhu, T.X., Band, L.E.,Vertessy, R.A. (1999). Continuous modeling of intermittent stormflows on a semi-arid agricultural catchment. *Journal of Hydrology 226,* 11-29.

Zhu, T. X., Luk, S. H., Cai, Q. G. (2002). Tunnel erosion and sediment production in the hilly loess region, North China. *Journal of Hydrology 257,* 78-90.

INDEX OF FIGURES

INDEX OF TABLES

GPS Point Regression - Parameters

2.5 m

Site	Elevation	A	+/-	B	+/-	$\nabla^2 z$	+/-	D	+/-	E	+/-	∇z	+/-
S1	73,01	0,0050	0,0030	0,0037	0,0029	0,0173	0,0116	-0,0216	0,0038	-0,0134	0,0036	0,0254	0,0051
S2	72,18	-0,0140	0,0053	-0,0097	0,0040	-0,0475	0,0187	-0,0382	0,0071	-0,0778	0,0059	0,0867	0,0084
S3	71,07	-0,0039	0,0050	-0,0150	0,0057	-0,0377	0,0215	-0,0573	0,0060	-0,1335	0,0068	0,1453	0,0086
S4	66,28	-0,0077	0,0059	-0,0185	0,0079	-0,0523	0,0276	-0,0187	0,0083	-0,2425	0,0093	0,2432	0,0098
S5	59,53	-0,0506	0,0103	-0,0521	0,0098	-0,2054	0,0402	-0,1119	0,0114	-0,3313	0,0114	0,3497	0,0144

5.0 m

	A	+/-	B	+/-	$\nabla^2 z$	+/-	D	+/-	E	+/-	∇z	+/-
S1	0,0007	0,0004	0,0001	0,0005	0,0017	0,0018	-0,0210	0,0011	-0,0123	0,0011	0,0243	0,0015
S2	-0,0023	0,0007	-0,0033	0,0007	-0,0112	0,0027	-0,0454	0,0017	-0,0729	0,0017	0,0859	0,0023
S3	-0,0010	0,0006	-0,0048	0,0006	-0,0117	0,0025	-0,0533	0,0016	-0,1258	0,0015	0,1366	0,0020
S4	-0,0025	0,0011	-0,0057	0,0010	-0,0164	0,0041	-0,0350	0,0025	-0,2447	0,0023	0,2471	0,0026
S5	-0,0386	0,0016	-0,0167	0,0018	-0,1107	0,0067	-0,1221	0,0037	-0,3226	0,0039	0,3449	0,0049

7.5 m

	A	+/-	B	+/-	$\nabla^2 z$	+/-	D	+/-	E	+/-	∇z	+/-
S1	0,0004	0,0002	-0,0005	0,0001	-0,0001	0,0007	-0,0181	0,0006	-0,0105	0,0005	0,0209	0,0008
S2	-0,0017	0,0002	-0,0022	0,0002	-0,0078	0,0009	-0,0450	0,0008	-0,0696	0,0008	0,0829	0,0011
S3	-0,0013	0,0003	-0,0042	0,0002	-0,0110	0,0011	-0,0535	0,0010	-0,1202	0,0008	0,1316	0,0012
S4	-0,0020	0,0005	-0,0064	0,0004	-0,0168	0,0017	-0,0316	0,0016	-0,2495	0,0014	0,2515	0,0016
S5	-0,0308	0,0007	-0,0076	0,0008	-0,0769	0,0030	-0,0960	0,0025	-0,3264	0,0027	0,3402	0,0032

10.0 m

	A	+/-	B	+/-	$\nabla^2 z$	+/-	D	+/-	E	+/-	∇z	+/-
S1	-0,0002	0,0001	-0,0012	0,0001	-0,0028	0,0004	-0,0184	0,0006	-0,0108	0,0004	0,0214	0,0007
S2	-0,0013	0,0001	-0,0015	0,0001	-0,0056	0,0005	-0,0444	0,0006	-0,0671	0,0005	0,0805	0,0007
S3	-0,0017	0,0002	-0,0038	0,0001	-0,0110	0,0006	-0,0525	0,0009	-0,1206	0,0006	0,1315	0,0009
S4	-0,0012	0,0004	-0,0060	0,0003	-0,0144	0,0012	-0,0261	0,0018	-0,2578	0,0013	0,2591	0,0014
S5	-0,0180	0,0007	-0,0028	0,0007	-0,0416	0,0027	-0,0888	0,0032	-0,3330	0,0031	0,3446	0,0038

15.0 m

	A	+/-	B	+/-	$\nabla^2 z$	+/-	D	+/-	E	+/-	∇z	+/-
S1	-0,0006	0,0001	-0,00116	0,00004	-0,0035	0,0002	-0,0184	0,0005	-0,0119	0,0003	0,0219	0,0006
S2	-0,0012	0,0001	-0,00190	0,00004	-0,0062	0,0003	-0,0437	0,0005	-0,0695	0,0003	0,0821	0,0005
S3	-0,0012	0,0001	-0,00289	0,00004	-0,0082	0,0003	-0,0458	0,0011	-0,0597	0,0010	0,0752	0,0015
S4	-0,0010	0,0002	-0,0050	0,0001	-0,0120	0,0007	-0,0245	0,0019	-0,2657	0,0009	0,2668	0,0011
S5	-0,0056	0,0005	0,0002	0,0004	-0,0108	0,0018	-0,0644	0,0035	-0,3394	0,0035	0,3454	0,0041

$\nabla^2 z$ ... Curvature: 2*(A+B)
∇z ... Gradient: SQRT (D^2+E^2)
A, D ... Plan parameters
B, E ... Profile parameters

^{137}Cs - Areal Activity

Site	ρ_B*	+/-	Activity	+/-	Areal Activity**	+/-
	[g/cm³]		[Bq/kg]		[Bq/m²]	
IF 1-4						
0 - 10	0,61	0,04	3,12	0,37	189	35
10 - 20	0,89	0,06	0,60	0,18	53	20
20 - 30	1,21	0,08	0,65	0,20	79	30
30 - 40	1,57	0,11	0,39	0,16	61	29
				Total:	**382**	**114**
IF 5-8						
0 - 10	0,83	0,06	3,25	0,39	271	51
10 - 40	1,19	0,08	0,29	0,29	208	14
				Total:	**479**	**65**
S1						
0 - 10	0,79	0,05	3,31	0,56	263	62
10 - 40	1,44	0,10	0,58	0,21	250	108
				Total:	**513**	**170**
S2						
0 - 10	0,75	0,05	3,74	0,62	280	65
10 - 40	1,41	0,10	0,34	0,34	288	20
				Total:	**568**	**85**
S3						
0 - 10	0,82	0,06	3,15	0,54	260	62
10 - 40	1,43	0,10	0,78	0,24	334	126
				Total:	**594**	**188**
S4						
0 - 10	1,14	0,08	1,84	0,38	210	58
10 - 40	1,48	0,10	0,32	0,32	281	19
				Total:	**491**	**77**
S5						
0 - 10	1,18	0,08	2,12	0,39	251	63
10 - 40	1,62	0,11	0,32	0,32	311	21
				Total:	**562**	**84**

* assumes sample volume 610 +/- 40 cm³

** Areal Activity is calculated as ρ_B x Activity

Sample Spiking

Site	Depth increment [cm]	ρ_B [g/cm^3]	Subsample Mass [g]	Subsample 'Treated'** [g]	Spike Weight [g]	Spike Concentr.	Number Grains	Number Spikes	Glass Conc. Clean Soil [glass/g]	Glass Conc. Increment [glass/g]	Glass Conc. Aereal glass/cm²
S1	0 - 10	0.72	26.51	2.73	0.13	0.05	1	71	478	21,557	2,450
	10 - 20	0.97	61.93	2.57	0.13	0.05	2	46	1,431	35,032	3,981
	20 - 30	1.23	21.07	1.91	0.09	0.05	2	51	1,348	91,678	10,418
	30 - 40	1.36	20.51	2.05	0.10	0.05	4	51	2,622	217,230	24,685
	40 - 50	1.79	25.06	2.28	0.12	0.05	4	74	1,834	181,408	20,615
	50 - 60	2.15	44.44	5.91	0.29	0.05	4	65	2,031	353,417	40,161
	60 - 70	2.20	48.27	15.23	0.75	0.05	1	82	405	171,099	19,443
	70 - 80	2.12	49.47	10.78	0.53	0.05	6	68	2,957	831,122	94,446
	80 - 90	2.15	51.26	10.94	0.52	0.05	5	75	2,226	619,960	70,450
	90 - 100	1.86	48.55	8.15	0.40	0.05	5	96	1,724	326,552	37,108
	100 - 110	1.82	59.53	7.05	0.35	0.05	3	80	1,267	165,759	18,836
	110 - 120	1.90	23.64	3.55	0.19	0.05	2	69	1,009	174,701	19,852
	120 - 130	1.86	22.09	3.97	0.20	0.05	6	74	2,761	561,241	63,777
	130 - 140	1.90	25.14	3.62	0.18	0.05	3	50	1,985	329,660	37,461
	140 - 150	1.81	20.16	3.18	0.16	0.05	2	96	715	124,300	14,125
	150 - 160	1.87	21.71	6.00	0.30	0.05	9	82	3,693	1,159,339	131,743
	160 - 170	1.82	24.25	4.19	0.22	0.05	2	71	973	186,190	21,158
	170 - 180	1.78	20.25	3.33	0.17	0.05	8	85	3,137	560,235	63,663
	180 - 190	1.81	20.32	3.49	0.18	0.05	9	61	5,131	968,214	110,024
	190 - 200	1.64	23.10	5.76	0.29	0.05	9	103	2,984	743,276	84,463
	200 - 210	1.71	20.91	4.69	0.24	0.05	1	67	517	120,878	13,736
	210 - 220	1.84	22.40	3.29	0.17	0.05	5	80	2,171	356,548	40,517
	220 - 230	1.51	24.89	3.27	0.16	0.05	9	90	3,306	399,640	45,414
	230 - 240	1.91	20.03	2.81	0.14	0.05	4	122	1,084	176,467	20,053
	240 - 250	1.89	20.45	3.31	0.17	0.05	0	83	0	0	0
	250 - 260	1.69	20.35	3.39	0.17	0.05	0	44	0	0	0
										Total:	1,008,580
S2	0 - 10	0.72	21.19	1.97	0.08	0.05	3	74	1,259	51,389	5,840
	10 - 20	1.10	12.60	1.01	0.05	0.05	3	48	1,991	106,973	12,156
	20 - 30	1.43	20.44	2.21	0.10	0.05	2	79	790	74,285	8,441
	30 - 40	1.58	21.13	1.81	0.10	0.05	0	71	0	0	0
	40 - 50	1.97	20.89	2.03	0.09	0.05	3	53	1,746	202,959	23,064
	50 - 60	1.98	21.17	3.92	0.19	0.05	5	46	3,542	789,467	89,712

	60 - 70	2.01	21.23	3.78	0.18	0.05	8	107	2,384	519,995	59,090
	70 - 80	2.14	21.05	4.14	0.20	0.05	4	56	2,280	582,921	66,241
	80 - 90	1.97	21.84	4.84	0.24	0.05	9	88	3,449	916,455	104,143
	90 - 100	1.93	23.05	4.18	0.21	0.05	0	48	0	0	0
	100 - 110	1.77	22.85	4.26	0.22	0.05	7	81	2,972	595,251	67,642
	110 - 120	1.79	21.99	2.86	0.14	0.05	17	81	6,756	955,973	108,633
	120 - 130	1.81	20.78	2.69	0.13	0.05	12	88	4,518	644,842	73,277
	130 - 140	1.90	22.30	2.87	0.14	0.05	18	51	11,830	1,756,537	199,607
	140 - 150	1.96	22.65	3.04	0.14	0.05	32	50	20,360	3,259,707	370,421
	150 - 160	1.83	20.31	2.70	0.12	0.05	80	45	53,303	7,866,267	893,894
	160 - 170	1.58	20.85	3.02	0.15	0.05	153	120	41,959	5,856,315	665,490
	170 - 180	1.63	20.27	3.12	0.15	0.05	168	59	91,810	14,002,997	1,591,250
	180 - 190	1.72	21.66	3.36	0.16	0.05	42	45	30,259	4,902,360	557,086
	190 - 200	1.63	20.42	3.40	0.16	0.05	12	60	6,384	1,051,316	119,468
	200 - 210	1.63	22.26	5.71	0.27	0.05	4	39	3,262	828,785	94,180
										Total:	5,109,636
S3	0 - 10	0.51	14.58	1.59	0.07	0.05	7	112	2,219	300,648	34,165
	10 - 20	1.21	3.30	0.24	0.02	0.08	4	120	1,819	388,206	44,114
	20 - 30	1.45	21.97	1.80	0.08	0.05	3	70	1,334	384,943	43,743
	30 - 40	1.63	20.69	1.76	0.12	0.07	0	50	0	0	0
	40 - 50	2.00	23.36	2.21	0.11	0.05	2	102	639	73,535	8,356
	50 - 60	2.00	21.43	2.41	0.11	0.05	5	84	1,794	245,549	27,903
	60 - 70	2.09	21.10	2.23	0.11	0.05	4	76	1,782	239,834	27,254
	70 - 80	1.99	20.25	2.53	0.12	0.05	1	121	268	40,450	4,597
	80 - 90	2.08	23.97	3.01	0.14	0.05	4	68	1,878	298,323	33,900
	90 - 100	1.95	20.02	2.41	0.12	0.05	2	109	598	85,506	9,717
	100 - 110	1.92	20.90	2.58	0.13	0.05	5	59	2,776	400,225	45,480
	110 - 120	1.67	20.81	2.62	0.14	0.05	17	133	4,423	567,134	64,447
	120 - 130	1.78	21.69	2.94	0.16	0.05	33	109	10,598	1,559,507	177,217
	130 - 140	1.82	20.51	2.75	0.12	0.04	11	64	4,958	736,880	83,736
	140 - 150	1.87	20.32	2.83	0.14	0.05	13	47	9,069	1,438,054	163,415
	150 - 160	1.84	20.60	3.06	0.17	0.05	115	62	67,274	11,192,274	1,271,849
	160 - 170	1.90	24.46	4.53	0.21	0.05	174	119	45,987	9,863,324	1,120,832
	170 - 180	1.80	20.49	3.85	0.19	0.05	13	45	9,321	1,913,917	217,491
	180 - 190	1.47	20.44	4.48	0.23	0.05	2	79	854	167,507	19,035
	190 - 200	1.92	21.54	4.11	0.20	0.05	0	80	0	0	0
										Total:	3,397,252

S4	0 - 10	0.99	21.15	2.09	0.09	0.04	4	44	2,717	162,459	18,461
	10 - 20	1.25	22.33	1.89	0.09	0.05	1	70	493	31,618	3,593
	20 - 30	1.65	22.64	2.00	0.09	0.05	1	50	635	56,295	6,397
	30 - 40	1.69	23.19	2.20	0.10	0.05	3	60	1,545	150,393	17,090
	40 - 50	1.79	20.40	1.82	0.10	0.05	7	84	3,034	293,999	33,409
	50 - 60	1.96	20.07	2.31	0.13	0.06	4	68	2,159	296,743	33,721
	60 - 70	1.89	20.31	2.21	0.11	0.05	30	116	8,328	1,043,818	118,616
	70 - 80	1.86	21.71	2.88	0.14	0.05	25	80	9,903	1,489,067	169,212
	80 - 90	1.96	21.31	2.53	0.13	0.05	18	43	13,853	1,957,353	222,427
	90 - 100	1.97	21.97	3.12	0.16	0.05	49	81	20,581	3,497,006	397,387
	100 - 110	2.00	20.18	2.91	0.15	0.05	18	184	3,381	592,935	67,379
	110 - 120	2.00	24.12	3.94	0.21	0.05	1	98	356	70,806	8,046
	120 - 130	1.78	23.87	3.70	0.20	0.05	0	139	0	0	0
	130 - 140	1.90	20.65	2.90	0.15	0.05	0	90	0	0	0
										Total:	1,095,738
S5	0 - 10	1.19	13.83	1.55	0.08	0.05	3	77	1,358	109,896	12,488
	10 - 20	1.39	53.48	5.68	0.28	0.05	3	61	1,585	142,528	16,196
	20 - 30	1.55	21.41	2.60	0.12	0.05	1	96	339	38,800	4,409
	30 - 40	1.79	21.15	2.27	0.12	0.05	1	85	401	47,037	5,345
	40 - 50	1.60	24.11	3.51	0.19	0.05	1	90	390	55,316	6,286
	50 - 60	2.07	21.31	3.32	0.17	0.05	2	133	504	98,888	11,237
	60 - 70	2.02	20.23	3.27	0.16	0.05	3	58	1,734	344,619	39,161
	70 - 80	1.86	20.37	3.29	0.17	0.05	1	90	387	70,907	8,058
	80 - 90	1.95	24.80	3.64	0.18	0.05	0	75	0	0	0
	90 - 100	1.89	20.47	2.82	0.14	0.05	0	106	0	0	0
	100 - 110	1.92	20.92	3.12	0.15	0.05	0	91	0	0	0
	110 - 120	1.77	20.82	3.64	0.18	0.05	1	125	260	48,894	5,556
	120 - 130	1.80	20.39	3.39	0.18	0.05	0	78	0	0	0
										Total:	108,737

* assumes sample volume 610 +/- 40 cm^3

** assumes 664,800 grains/g of spike

Soil profile Ahuriri quarry (Source: Shanhun, 2004)

Location: Ahuriri loess quarry
Map Reference: NZMS 260 2476405 5722764
Mean Annual Rainfall: 690 mm yr^{-1}

Date described: 21/10/2003
Author(s): PCA, LJH, FLS

Bw(f)	0 - 17 cm	silt loam; 2.5Y 6/3 (light brownish grey to light yellowish brown); few fine distinct 7.5YR 3/4 (dark brown) mottles; very firm soil strength, brittle failure, weak coarse blocky structure; clear smooth boundary.
Bt(f)	17 - 30 cm	clay loam; 2.5Y 6/3 (light brownish grey to light yellowish brown); many coarse distinct 7.5YR 5/6 (strong brown) mottles; strong soil strength, brittle failure, moderate medium prismatic structure; gradual boundary.
Bx	30 - 155 cm	silt loam to loamy fine sand with depth; 2.5Y 5/3 (greyish brown to light olive brown); strong soil strength, brittle failure, moderate gross prismatic structure; clear boundary; Note: Some prisms up to 30 cm in diameter. Lower part of horizon has is 5Y 6/3 with fine colour segregations of 2.5Y 5/3.
2C	155 - 188 cm	loamy fine sand; 5Y 6/2 (light olive grey); moderately firm soil strength, brittle failure, massive; abrupt boundary.
3BCt	188 - 197 cm	silt loam; 2.5Y 5/4 (light olive brown); strong soil strength, brittle failure, massive; abrupt boundary; Note: 1-3 mm laminated sand (5Y 6/2(and loamy fine sand (2.5Y 5/4). In places just pods of sand; fine worm castings..
4C	197 - 206 cm	loamy fine sand; 5Y 5/3 (olive); slightly firm soil strength, brittle failure, massive; abrupt boundary.
5C	206 - 245 cm	loamy fine sand; 5Y 6/2 (light olive grey) and 2.5Y 6/4 (light yellowish brown); very firm soil strength, brittle failure, massive; abrupt boundary; Note: Vermiform fabric.

6C(k)	245 - 263 cm	loamy fine sand; 5Y 5/3 (olive); strong soil strength, brittle failure, massive; few fine filamentous carbonate; abrupt boundary.
7Ck1	263 - 296 cm	fine sandy loam; 5Y 6/2 (light olive grey); moderately firm soil strength, brittle failure, massive; common coarse filamentous carbonate; gradual boundary; Note: Halos of browner colour occur around grey sandy centers.
7Ck2	296 - 360 cm	fine sandy loam; 5Y 6/2 (light olive grey); moderately firm soil strength, brittle failure, massive; few fine filamentous carbonate; abrupt boundary; Note: some variogation of colour.
8BCt(k)	360 - 365 cm	loamy fine sand; 5Y 6/2 (light olive grey) and 2.5Y 5/4 (light olive brown); strong soil strength, brittle failure, massive; few fine filamentous carbonate; abrupt boundary.
9C(k)	365 - 385 cm	fine sand; 5Y 6/2 (light olive grey); few extr. fine faint 10YR 4/2 (dark greyish brown) mottles; moderately firm soil strength, brittle failure, massive; few fine filamentous carbonate; .
10BCt	385 - 397 cm	silt loam; 2.5Y 6/3 (light brownish grey to light yellowish brown) and 5Y 7/2 (light grey); common extr. fine faint 10YR 4/2 (dark greyish brown) mottles; strong soil strength, brittle failure, massive; few very fine filamentous carbonate; abrupt boundary; Note: Carbonate is absent by the base of the horizon.
11C	397 - 470 cm	silt loam; 5Y 6/3 (pale olive); 10YR 4/2 (dark greyish brown) mottles; strong soil strength, brittle failure, massive; irregular boundary.
12Bwk1	470 - 497 cm	silt loam; 2.5Y 4/3 (dark greyish brown to olive brown); strong soil strength, brittle failure, massive; many coarse filamentous ped face coatings; gradual boundary; Note: Hackley broken surface and strong vermiform fabric.

12Bw(k)2	497 - 530 cm	silt loam; 2.5Y 4/3 (dark greyish brown to olive brown); strong soil strength, brittle failure, massive; few fine filamentous ped face coatings; ; Note: Hackley broken surfaces and vermiform fabric.
13C	530 - 555 cm	loamy fine sand; 5Y 7/2 (light grey); weak soil strength, brittle failure, massive; few fine (< 2 mm) filamentous carbonate; sharp broken boundary; Note: Carbonate appears in browner, finer textured pods.
14Bw	555 - 595 cm	silt loam; 2.5Y 4/2 (dark greyish brown) and 2.5Y 7/2 (light grey); common extr. fine distinct 7.5YR 4/4 (brown) mottles; very firm soil strength, brittle failure, massive; gradual boundary; Note: No carbonate.
14Bw(k)	595 - 630 cm	silt loam; 2.5Y 5/3 (greyish brown to light olive brown); moderately firm soil strength, brittle failure, massive to weak gross prismatic structure; few fine filamentous carbonate; ; Note: Carbonate also occurs as nodules forming in cracks - this carbonate was sampled. Vermiform fabric.

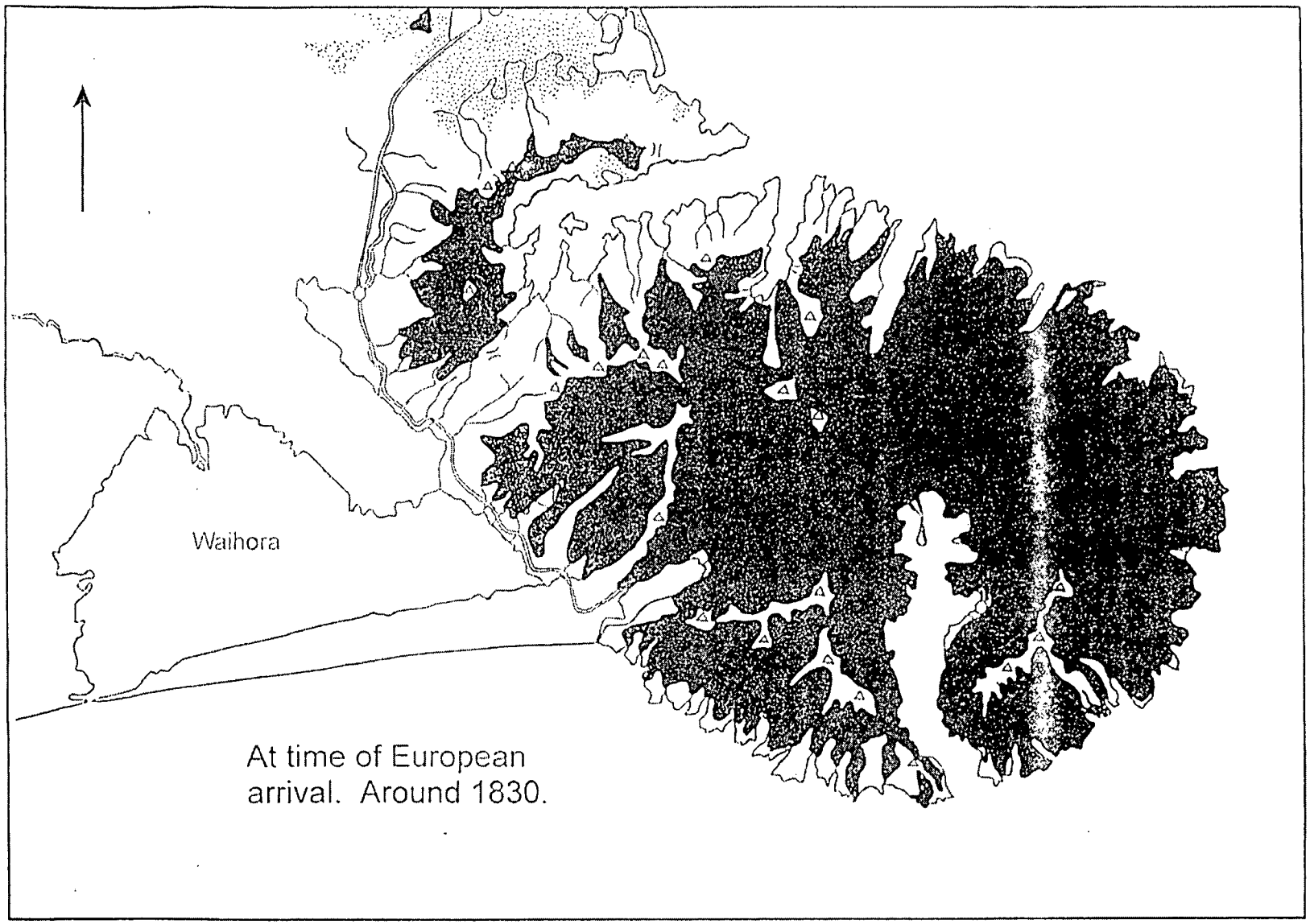

Fig. 4 Probable extent of forest on Banks Peninsula around 1830 just before the beginning of European settlement (based on current field evidence and maps in Johnston (1961) and Petrie (1963)).

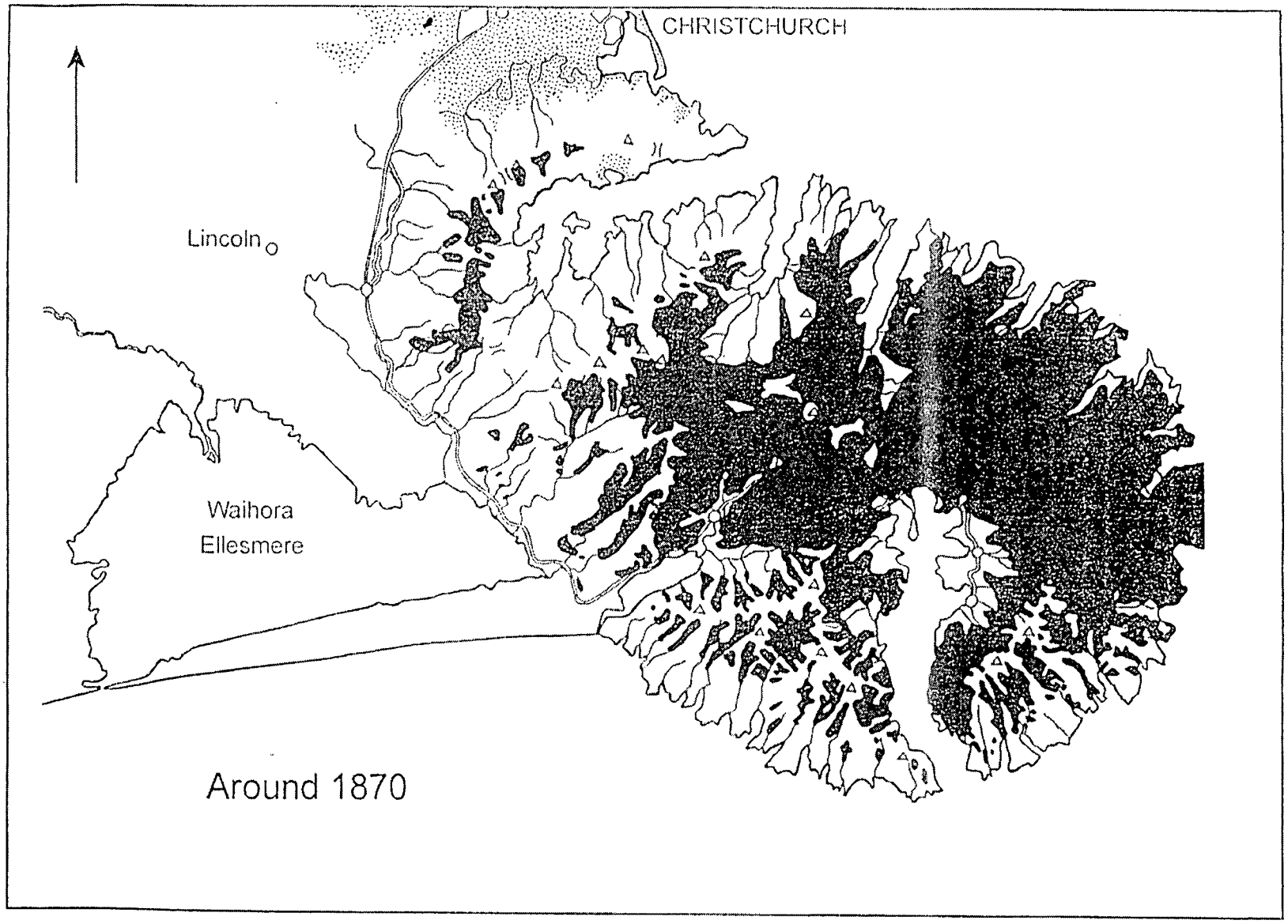

Fig. 5 Approximate extent of forest on Banks Peninsula around 1870 (based on Johnston, 1961).

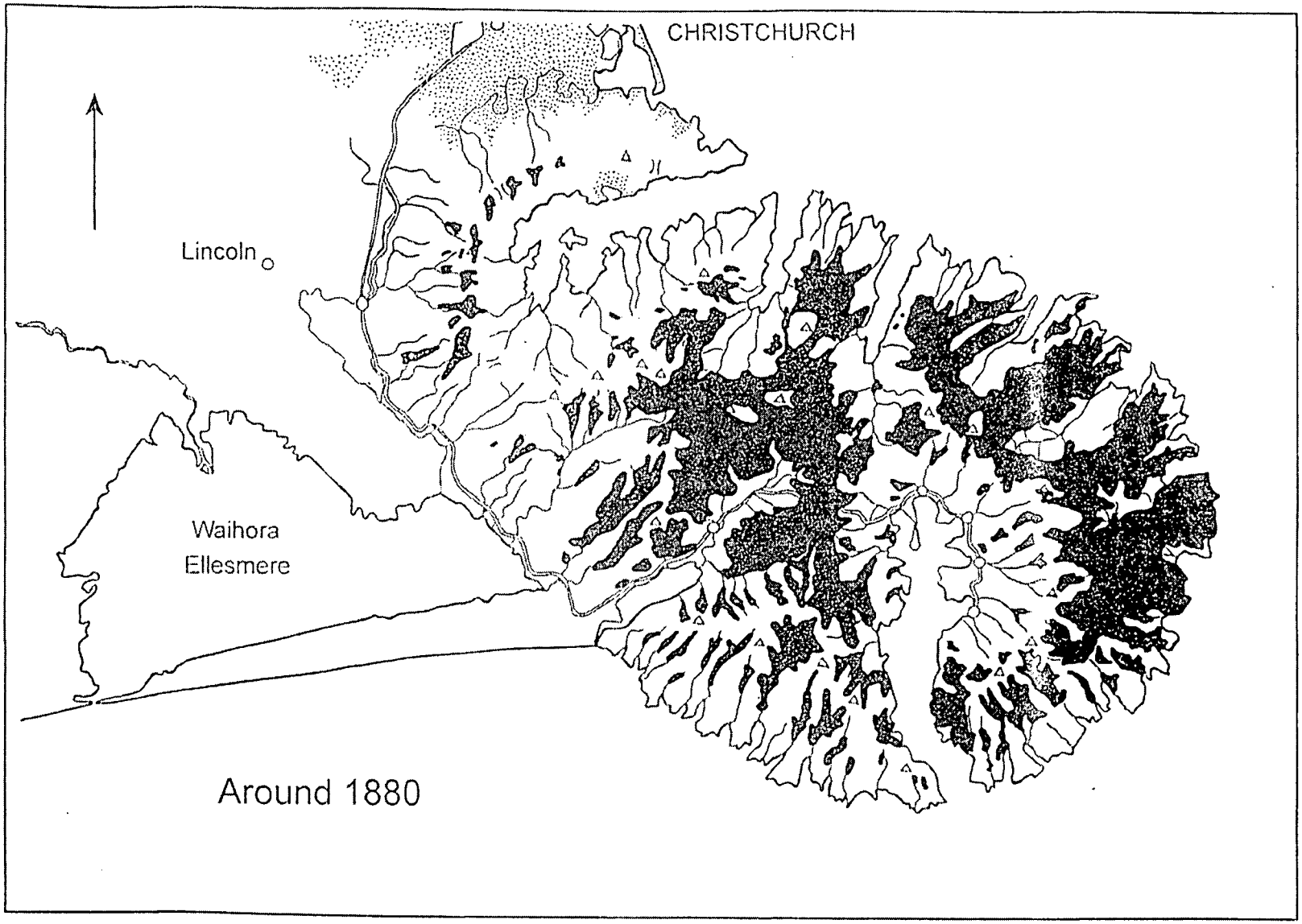

Fig. 6 Approximate extent of forest on Banks Peninsula around 1880 (based on Petrie, 1963).

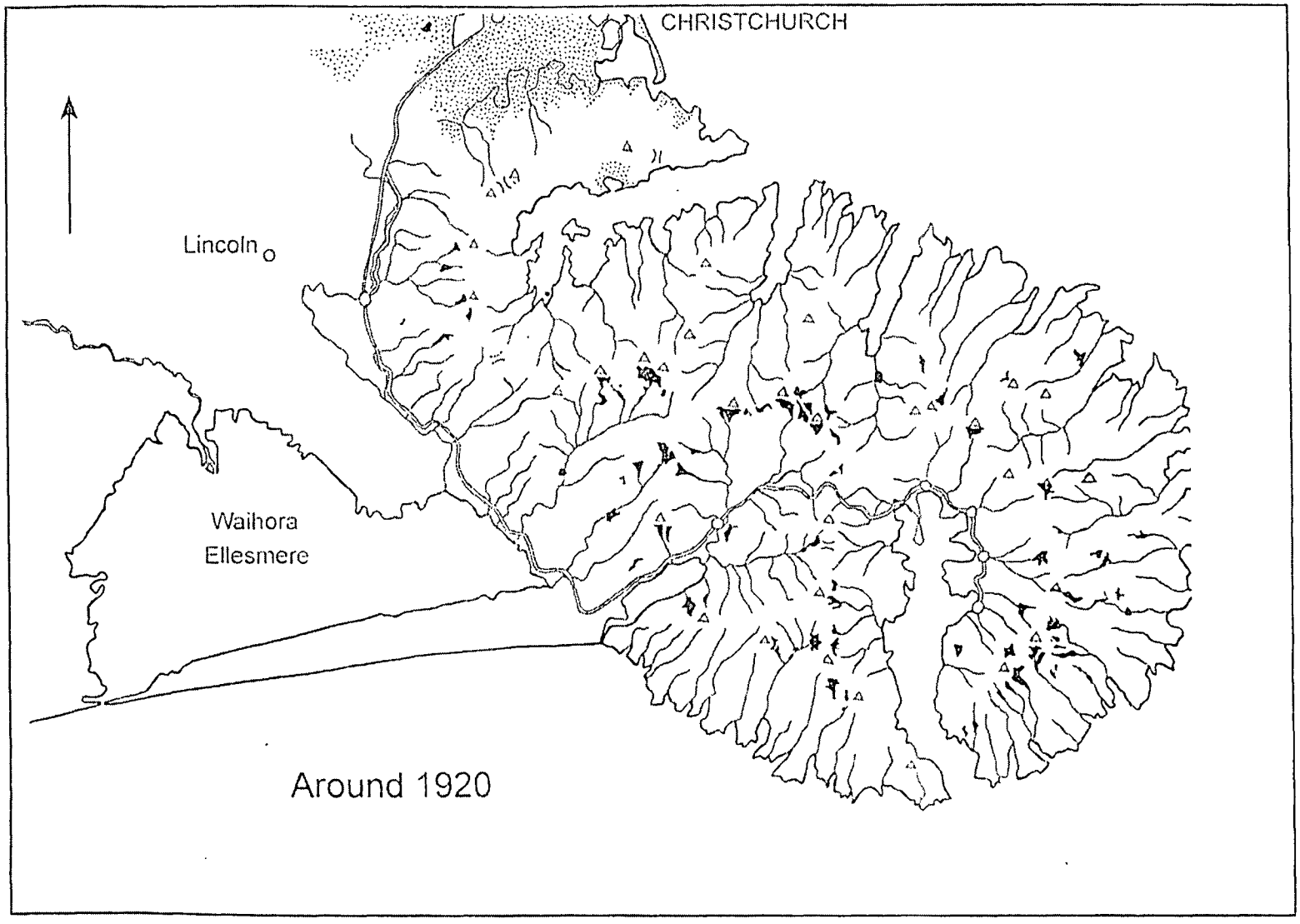

Fig.ure 7 Approximate extent of native forest following the cessation of milling in the 1920s (based on numerous historical photos, records and current field evidence). The last mills operated at Port Levy and above Pigeon Bay (Ogilvie, 1990).

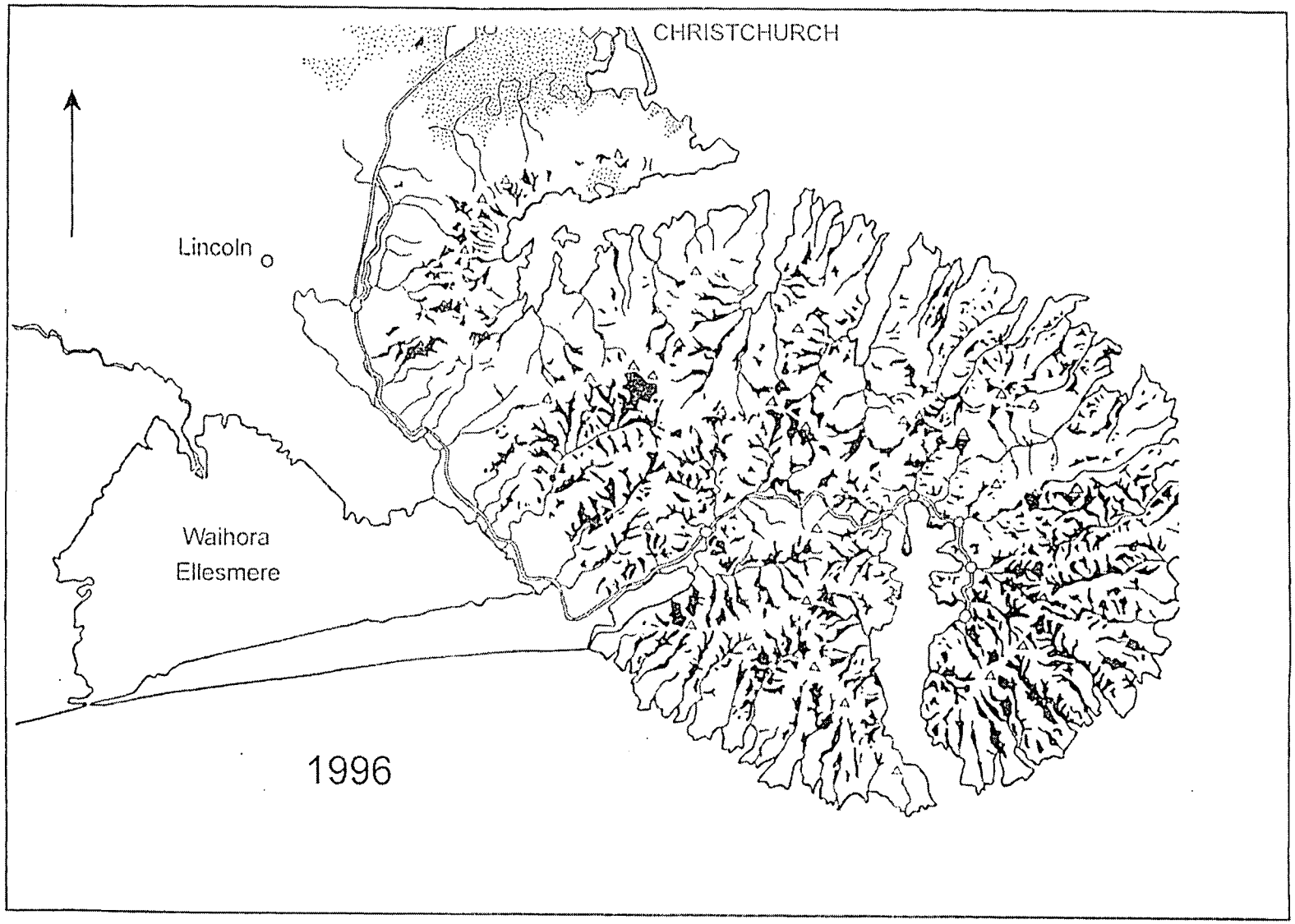

Fig. 8 Extent of native forest, 1996 (based on aerial photography and detailed fieldwork on the ground, Wilson, 1993). Exotic plantation forest is not shown, but in 1996 occupied almost two percent of the Peninsula's area.

Regression Statistics	
Multiple R	0.87
R Square	0.75
Adj. R Square	0.25
Standard Error	0.30
Observations	3

ANOVA

	df	SS	MS	F	Significance F
Regression	1	0.53	0.53	6.03	0.25
Residual	2	0.17	0.09		
Total	3	0.70			

	Coefficients	Standard Error	t Stat	P-value	Lower 95%	Upper 95%	Lower 95.0%	Upper 95.0%
Intercept	0							
X Variable 1	-0.009	0.001	-7.31	0.018	-0.015	-0.004	-0.015	-0.004

Slope	h_0=-1/S	+/-
-0.009	109	15

Regression Statistics	
Multiple R	0.95
R Square	0.90
Adj. R Square	0.86
Standard Error	6.65E-06
Observations	4

ANOVA

	df	SS	MS	F	Significance F
Regression	1	8.33E-10	8.33E-10	18.82	0.05
Residual	2	8.85E-11	4.43E-11		
Total	3	9.21E-10			

	Coefficients	Standard Error	t Stat	P-value	Lower 95%	Upper 95%	Lower 95.0%	Upper 95.0%
Intercept	-1.30E-06	7.40E-06	-0.18	0.877	-3.31E-05	3.05E-05	-3.31E-05	3.05E-05
X Variable 1	-0.0032	0.0007	-4.34	0.049	-0.006	-2.59E-05	-0.006	-2.59E-05

K_{long}	+/-
0.0032	0.0007

Regression Statistics	
Multiple R	0.21
R Square	0.04
Adj. R Square	-0.27
Standard Error	3.76E-04
Observations	5

ANOVA

	df	SS	MS	F	Significance F
Regression	1	1.94E-08	1.94E-08	0.14	0.74
Residual	3	4.23E-07	1.41E-07		
Total	4	4.42E-07			

	Coefficients	Standard Error	t Stat	P-value	Lower 95%	Upper 95%	Lower 95.0%	Upper 95.0%
Intercept	0.0001	0.0002	0.65	0.5596	-0.0005	0.0008	-0.0005	0.0008
X Variable 1	-0.0008	0.0021	-0.37	0.735	-0.008	0.006	-0.008	0.006

K_{short}	+/-
-0.0008	0.0021